THE EFFECT OF TEMPERATURE AND PRESSURE ON THE LINEAR VISCOELASTIC RESPONSE OF ELASTOMERS

Thesis by

Robert W. Fillers

In Partial Fulfillment of the Requirements

for the Degree of

Doctor of Philosophy

California Institute of Technology

Pasadena, California

1975

(submitted July 19, 1974)

to Aline

ACKNOWLEDGEMENTS

I would like to take this opportunity to acknowledge those persons who have contributed to the completion of this thesis:

Especial thanks are extended to Professor N. W. Tschoegl who has consistently encouraged my intellectual discipline, broadened my research, and greatly contributed to my appreciation of the humanities. Both Dr. and Mrs. Tschoegl have extended the warmth of a personal friendship to each of the students and their wives, and for this, I am grateful.

I wish to thank both Professor R. W. Vaughan, for numerous suggestions regarding the initial design of the high pressure apparatus, and Dr. P. J. Blatz for many enlightening discussions concerning the analysis of the data.

I would like to express my good fortune in sharing an office with Vic Chang, who has consistently enriched my theoretical awareness of science. I am also fortunate in having established a warm friendship with Satish Sharda, with whom I have spent many pleasurable hours. The companionship and technical suggestions of Michio Okuyama are also deeply appreciated.

Thanks are due to Mrs. Eileen Finke for her secretarial assistance, and to George Griffith, whose technical skills and knowledge made many portions of the apparatus feasible.

I especially am grateful to Miss Rosalie Hernandez for typing this manuscript.

Finally, I wish to acknowledge my wife, Aline, for her patience and encouragement throughout the preparation of this thesis.

ABSTRACT

Stress relaxation measurements were made in uniaxial tension under superposed hydrostatic pressures up to 5 kbar at temperatures ranging from -25 to 50°C. Two lightly filled (Hypalon-40 and Viton-B) and one highly filled elastomer (Neoprene) were studied because their pressure transition lie within the range of the apparatus. The construction and operation of the apparatus are discussed. Measurements on Hypalon and Viton were made either by varying the temperature while maintaining the pressure constant at 1, 1,000, and 2,000 bars, or by holding the temperature constant while varying the pressure from atmospheric to 4,600 bars. The viscoelastic response of Neoprene was measured at 25°C and pressures up to 4,600 bars.

The measurements were converted to a time dependent shear modulus. Time-temperature and time-pressure superposition was then applied to the reduced data to obtain master curves at 1, 1,000, and 2,000 bars. By introducing either the Murnaghan or the Tait equation of state into the free volume theory, an expression was obtained which describes the shift factors, $\log a_{T,P}$, resulting from the empirical shifts into the master curves at atmospheric pressure. This equation then gave an excellent prediction of the empirically found shift factors resulting from forming the master curves at 1,000 and 2,000 bars.

Because the measurements made as function of temperature

and those made as a function of pressure must be consistent, certain ambiguities in the free volume theory have been removed. This leads to an essential improvement in the theory.

TABLE OF CONTENTS

LIST OF FIGURES

LIST OF TABLES

1. INTRODUCTION

Temperature and pressure are the two most important processing variables in polymer science and technology. While the effect of temperature on the mechanical properties of polymers (particularly amorphous polymers) is fairly well understood today, virtually no information is available on the effect of pressure. Introducing pressure as an independent variable not only adds another dimension to scientific observation and understanding, but fills a technological void as well.

Amorphous polymers exist as liquids or glasses depending upon the temperature, pressure, and time scale of observation. Elastomers, or rubbers, are amorphous polymers whose molecular chains are crosslinked into a three-dimensional network of randomly distributed, chemical or physical junctions. In the liquid (or rubbery) state there is sufficient molecular mobility so that long range molecular rearrangements may occur through cooperative segmental motion along the polymer chains. A measure of this molecular diffusion is the monomeric friction coefficient ζ_o which is a function of temperature and pressure. For a given temperature and pressure the magnitude of ζ_o determines the time required for cooperative rearrangements. When the observation time becomes shorter than the time required for cooperative rearrangements, the response of the system undergoes a transition from rubberlike to glasslike

behavior. In the glass, the configurational changes necessary for the maintenance of equilibrium essentially cease. The general molecular configuration existing when the glass is formed is essentially frozen in; the glass is considered to be unstable relative to some "metastable" equilibrium state which would result from an infinitely slow formation of the glass (1).

A polymer displays, simultaneously, both elastic and viscous response when subjected to external forces. In the rubbery state the elastic response is largely entropic, since the total number of configurations available to the amorphous system is reduced as a result of the deformation. The elastic response is reversible and represents energy storage in the system. As the glassy response is approached, the contribution from internal energy resulting mainly from changes in intermolecular attraction becomes the controlling mechanism. The viscous response results from the rearrangement of the molecular configuration, and is most pronounced in the transition region between the rubbery and glassy states. In this region the ratio of the imaginary to the real component of the viscoelastic response (i. e. the ratio of energy dissipation to energy storage) possesses a maximum. The viscous response is irreversible and represents energy dissipation in the system.

1.1 Phenomenological Theory of Viscoelastic Behavior

The basic hypothesis on which classical linear viscoelastic theory is based was first formulated in 1874 by Boltzmann (2). One form of Boltzmann's integral equation is

$$\sigma(t) = \int_{-\infty}^{t} Q(t-u)\ \epsilon(u)\ du \qquad (1)$$

where $\sigma(t)$ is the stress response at time t, $\epsilon(u)$ is the strain imposed at the previous (historic) time u, and $Q(t)$ is a weighting function corresponding to the time intervals $(t-u)$ which have elapsed since the imposition of the respective strains. The weighting function, or relaxance, is a material function which contains all the information necessary to completely describe the linear viscoelastic response of the material. The Boltzmann superposition principle is quite general and requires only that the relation between stress and strain be linear and time translation invariant, i.e. that it be described with linear differential equations with constant coefficients.

Viscoelastic behavior may be represented by spring and dashpot models. The Maxwell element is a Hookean spring in series with a Newtonian dashpot; viscoelastic behavior may then be represented by connecting many Maxwell elements in parallel to yield a distribution of responses (3). An additional spring is incorporated into the model to represent the equilibrium rubbery modulus. The generalized Maxwell model yields

$$G(t) = G_e + \sum_{p=1}^{N} G_p \exp(-t/\tau_p) \qquad (2)$$

where G(t) is the time dependent shear modulus, G_e is the equilibrium (or rubbery) modulus, and τ_p is the p'th relaxation time. The latter is equal to the quotient of the viscosity of the p'th dashpot, η_p divided by the shear modulus of the p'th spring, G_p. The generalized Maxwell model may be introduced into the Boltzmann integral for predicting linear viscoelastic response. Numerous variations of the spring-dashpot models exist (3). A more rigorous and generalized treatment of the phenomenological theory has been developed by Coleman and Noll (4) and reduces to the Boltzmann integral for small strains.

1.2 Molecular Theories of Viscoelastic Behavior

Various molecular theories have been developed for describing polymeric materials. The theories of Rouse (5) and Zimm (6) consider the behavior of a bead-and-spring model at infinite dilution. The Rouse theory has been extended to the undiluted system by Ferry, Landel and Williams (7), to yield the following expression for the shear modulus;

$$G(t) = \frac{\rho R T}{M} \sum_{p=1}^{N} \exp(-t/\tau_p) \qquad (3)$$

where

$$\tau_p = a^2 Z^2 \zeta_o / 6\pi^2 p^2 kT \tag{4}$$

or

$$\tau_p = 6\eta M / \pi^2 p^2 \rho RT \tag{5}$$

where ρ is the density, R is the gas constant, T is the temperature, and M is the molecular weight. The relaxation times are given in terms of η, the steady-flow shear viscosity, k the Boltzmann constant, ζ_o the monomeric friction factor, and a^2 the mean-square end-to-end distance per degree of polymerization, Z.

The front factor in Eq. (3) comes from the statistical theory of rubberlike elasticity and represents the equilibrium shear modulus. The statistical theory assumes that the polymer is flexible enough for its end-to-end distance to assume a Gaussian distribution. It is valid only above the glass transition, where the molecular rearrangements necessary for the minimization of the free energy may occur; the free energy is dominated by the configurational entropy of the flexible polymer chains. The rate of rearrangements, or relaxation times, predicted by the Rouse theory depend upon the steady-flow viscosity, η, or the monomeric friction factor ζ_o. A change in temperature affects both the rate of rearrangements and the value of the equilibrium modulus. Additionally, Eqs. (4) and (5) indicate that all relaxation times should be affected in a similar fashion by a change in temperature or pressure through the dependence of η, ζ_o and ρ on temperature and pressure.

1.3 Time-Temperature Superposition Principle

Complete characterization of the linear viscoelastic behavior of an elastomer requires measurements over 10 to 20 decades of time or frequency. Such a wide "experimental window" is virtually inaccessible. Thus, a major advancement in the rheology of amorphous polymers has been the utilization of time-temperature superposition; the time-temperature superposition principle was originally proposed by Leaderman (8), applied by Tobolsky (9), and finally given a theoretical interpretation by Ferry and co-workers (10). It states that the general effect of temperature on the rate of molecular rearrangement is to multiply all relaxation times by a common factor, usually designated a_T. This factor is defined as the ratio of a particular relaxation time at temperature T to that of a reference temperature T_o,

$$a_T = \tau_p(T)/\tau_p(T_o) \tag{6}$$

where $\tau_p(T)$ is the p'th relaxation time at temperature T. A material satisfying this criterion is termed thermorheologically simple.

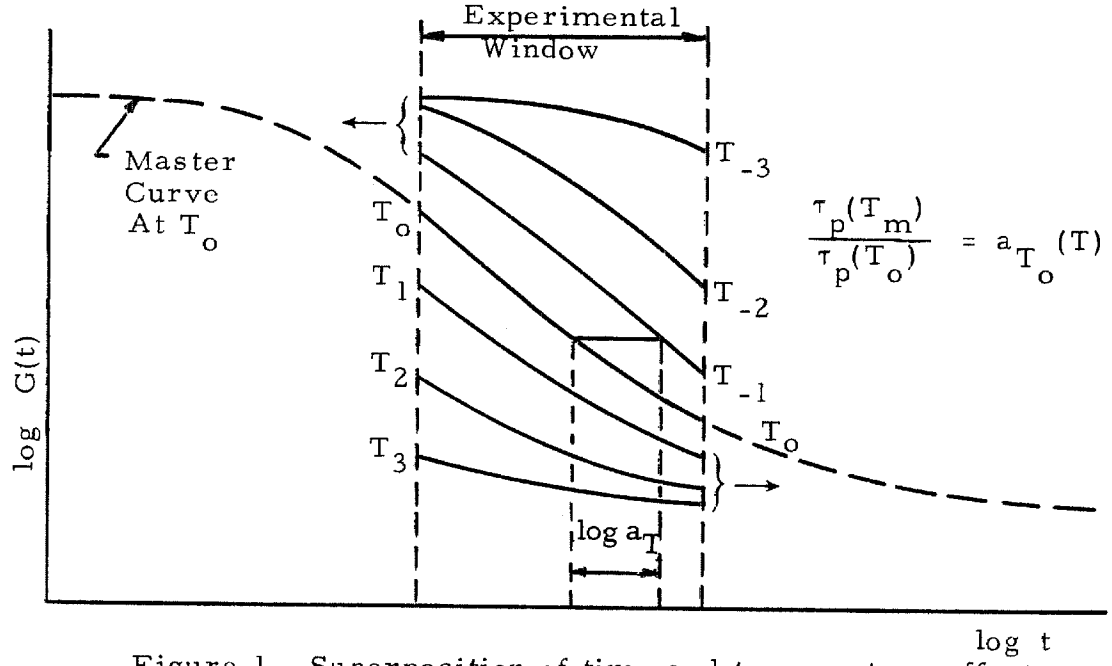

Figure 1. Superposition of time and temperature effects.

Time-temperature superposition is depicted diagrammatically in Fig. 1, where values of the shear modulus G(t) are shown over the experimentally accessible time regime (the experimental window) at a series of temperatures, T_{-3} to T_3. The horizontal shift along the logarithmic time axis required to superpose log G(t) at various temperatures into a single master curve at the reference temperature T_o is $\log a_{T_o}(T) = \log a_T$. Thus, experimental information over a limited time regime, but covering a range of temperatures, has been shifted in logarithmic time to describe the material response at a single reference temperature, but covering a significantly expanded time scale.

The reduced modulus $G^{T_o}(t/a_T)$ resulting from the superposition is related to the original moduli through the relation

$$G^{T_o}(t/a_T) = d_T G^T(t) \tag{7}$$

where

$$d_T = \rho_o T_o / \rho_T T \tag{8}$$

The expression for d_T results from the statistical theory of rubberlike elasticity and therefore requires that both T and T_o be above the glass transition, where the configurational entropy dominates. As the glassy response is approached, the internal energy contribution to the total free energy of the system becomes increasingly more significant and eventually becomes the controlling mechanism.

A more general development of time-temperature superposition by McCrum and Morris (11, 12) suggests that

$$G^{T_o}(t/a_T) = \frac{c_T}{d_T}\left[d_T G^T(t) - G_r{}^{T_o} \right] + G_r{}^{T_o} \tag{9}$$

where

$$c_T = G_u{}^{T_o} / G_u{}^T \tag{10}$$

and

$$d_T = G_r{}^{T_o} / G_r{}^T \tag{11}$$

where $G_u{}^T$, $G_r{}^T$ and $G_u{}^{T_o}$, $G_r{}^{T_o}$ are the limiting unrelaxed and relaxed (r) shear moduli at temperature T and the reference temperature T_o. The above expression reduces to Eq. (7) by choosing c_T equal to unity and d_T as defined in Eq. (8). Unfortunately,

the relaxed and unrelaxed moduli at each temperature are experimentally unobtainable within the confines of the experimental window through which measurements are being made (if they were, time-temperature superposition would not be necessary). However, this expression does indicate that in the glassy region, additional adjustments should be made to the magnitude of the moduli where the statistical theory is no longer valid.

Uncrosslinked polymers do not exhibit equilibrium properties. However, measurements of the steady-flow viscosity as a function of temperature should also yield the temperature dependence of a_T. Molecular theory, Eqs. (5) and (6), predict that the viscosity should be related to a_T by the relation

$$a_T = \frac{\eta T_o \rho_o}{\eta_o T \rho_T} \tag{12}$$

The functional dependence of a_T determined from viscosity measurements is found to correlate quite well with viscoelastic measurements.

The effect of temperature on the viscosity of liquids has been widely studied. As early as 1920, Vogel (13) and Tamman and Hesse (14) proposed the empirical equation

$$\ln \eta = A_v + \frac{B_v}{T - T_\infty} \tag{13}$$

where A_v and B_v are constants, and T_∞ is a reference temperature at which the viscosity becomes infinite. An Arrhenius type relation

$$\eta = A\exp(\Delta H_a/RT) \tag{14}$$

was later proposed by Andrade in 1930, and subsequently given a theoretical interpretation, in the liquid state, by Eyring (15). In the absolute rate theory of Eyring, ΔH_a and A are, respectively, the enthalpy and entropy of activation for viscous flow. Combining Eqs. (12) and (14) yields

$$\log a_T = \frac{\Delta H_a}{2.303\,R}\left(\frac{1}{T} - \frac{1}{T_o}\right) + \log\frac{T_o\rho_o}{T\rho} \tag{15}$$

which is found to describe the viscosity in both glasses and liquids ($T < T_g + 100^oC$); values of ΔH_a vary from between 5 to 30 kcal/mole.

If the Vogel equation is introduced into Eq. (12), and the effects of T and ρ in Eq. (12) are neglected, we have

$$\log a_T = \frac{-c_1^{\,o}(T - T_o)}{c_2^{\,o} + T - T_o} \tag{16}$$

where

$$c_1^{\,o} = B_v/2.303\,(T_o - T_\infty) \tag{17}$$

$$c_2^{\,o} = T_o - T_\infty \tag{18}$$

This equation was proposed by Williams, Landel and Ferry in 1955

and is known as the WLF equation (10). It is found to predict the temperature dependence of viscous and viscoelastic behavior, of both polymers and other glass forming systems, over the temperature range of $T_g < T < T_g + 100^oC$. If the reference temperature T_o is chosen to be the glass transition temperature T_g, the constants become c_1^g and c_2^g, and are nearly the same for most polymers. This implies that the temperature dependence of molecular mobility is nearly independent of molecular structure; the primary effect of temperature is on the mechanisms controlling molecular mobility.

1.4 Free Volume Theory of the Temperature Dependence of Viscoelastic Behavior

The classical approaches to studying the vitrification process have been viscometric and volumetric measurements as a function of temperature. Viscosity plotted against temperature results in a curve quite similar to the master curve shown in Fig. 1, with the ordinate being log η and the abscissa being T; the inflection point of the transition region is usually within a few degrees of T_g. Volumetric measurements yield the thermal expansivity α as a function of temperature. The thermal expansivity is usually linear above and below the glass transition as shown in Fig. 2. Experimentally the thermal expansivity changes smoothly from the expansivity of the rubber, α_r, to the expansivity of the glass α_g; the intersection of the extrapolated linear values are taken to be

T_g. It is a natural consequence of such measurements that the molecular mobility in the rubbery (or liquid) state be attributed to the additional, or "excess", volume. This approach was first used by Batchinski (16) for describing the viscosities of liquids.

In 1951 Doolittle (17) proposed an empirical equation for the viscosity dependence on the excess, or free, volume;

$$\eta = A_f \exp(B_f V_\phi / V_f) , \qquad V_\phi + V_f = V \tag{19}$$

where A_f and B_f are constants, and V_ϕ and V_f are the occupied and free volumes respectively. Conceptually, the dependence of η on the free volume assumes that the rate controlling step for viscous flow at low shear stresses is the formation of a void into which a molecular segment can jump. A simple, theoretical interpretation of this equation has been given by Turnbull and Cohen (18), by calculating the average diffusion rate of a hard, spherical molecule surrounded by a cage of nearest neighbor molecules. Fluctuations in density allow redistribution of the free volume without affecting the energy of the system. Transport occurs when the free volume reaches a critical volume V^*. Using standard statistical mechanics, the mean diffusion rate may be expressed in the form of the Doolittle equation; the Stokes-Einstein equation is then used to relate the mean diffusion rate to the shear viscosity. The thermal expansivity of the free volume is taken to be the difference between

the thermal expansions of the liquid and the glass ($\alpha_f = \alpha_l - \alpha_g$); the free volume thus defined is depicted in Fig. 2.

The free volume theory was expressed by Williams, Landel and Ferry (10) in terms of the fractional free volume.

$$f = \frac{V_f}{V} \approx \frac{V_f}{V_\phi} \tag{20}$$

They assumed a linear relationship

$$f = f_g + \alpha_f (T - T_g) \tag{21}$$

where

$$\alpha_f = \alpha_l - \alpha_\phi \qquad \text{for} \qquad T \geq T_g \tag{22a}$$

and

$$\alpha_f = \alpha_g - \alpha_\phi \qquad \text{for} \qquad T < T_g \tag{22b}$$

Here f_g is the fractional free volume at the glass transition, and α_l, α_g, and α_ϕ are the thermal expansivities of the liquid, glass, and occupied volumes respectively (it is common practice to let $\alpha_f = \Delta\alpha = \alpha_l - \alpha_g$). Combining Eqs. (12), (19), and (20) yields the WLF equation, where the coefficients are defined as

$$c_1^g = B_f/2.303f_g \tag{23a}$$

and

$$c_2^g = f_g/\alpha_f \tag{23b}$$

Or, in terms of the Vogel equation,

$$f_g = \frac{B_f}{B_v} (T_g - T_\infty) \tag{24a}$$

and

$$\alpha_f = B_f / B_v \tag{24b}$$

It is instructive to write the WLF equation in this form;

$$\log a_T = \frac{-B_f}{2.303 f_g} \cdot \frac{T - T_g}{f_g/\alpha_f + T - T_g} \tag{25}$$

Doolittle found B to be approximately unity for the low molecular weight liquids he studied. On this basis, the nearly universal values of c_1^g and c_2^g (-17.44^oC^{-1} and 51.6^oC, respectively) imply that f_g and α_f are of the order of 0.025 and $4.8 \times 10^{-4} {}^oC^{-1}$ respectively. However, it should be pointed out that the WLF equation is fairly sensitive to small changes in c_1^g and c_2^g. Furthermore, T_g is not well defined, nor are B_f, α_f and f_g. Thus there are considerable degrees of freedom in fitting experimental data to this equation. Simha and Boyer (19) have tabulated data on 14 polymers with T_g's ranging from 143 to 378^oK, and α_f ranging from 3.0 to $9.3 \times 10^{-4} {}^oC^{-1}$. This implies that either $\alpha_f \neq \Delta\alpha$, α_f varies considerably, or both. Interestingly enough they found the product $\Delta\alpha\, T_g$ to be nearly constant (0.113) for the materials studied. Based on this observation, they considered the glass transition to be an iso-free volume state; this approach had been proposed earlier by Fox and Flory (20). The iso-free volume approach leads to still another definition of f_g; the various definitions are shown

diagrammatically in Fig. 2. More detailed discussic of the various free volume approaches can be found in the re ws by Boyer (21), Kaelble (22), and Shen and Eisenberg (23).

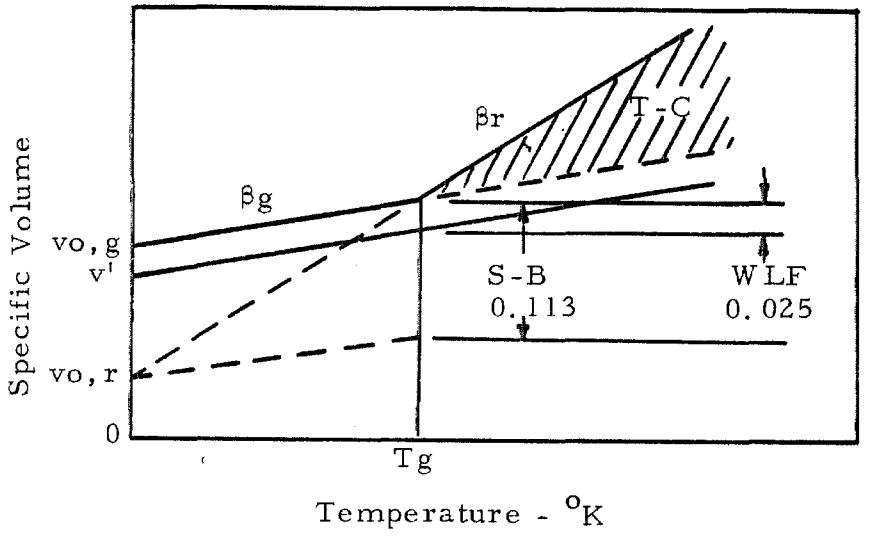

Figure 2. Free Volume as defined by Williams, Landel and Ferry (WLF), Simha and Boyer (S-B) and Turnbull and Cohen (T-C).

Two approaches to describing the temperature dependence of molecular mobility have been discussed. The rate theory of Eyring treats the probability of a molecule or segment obtaining sufficient energy to jump from one equilibrium position to an adjacent site. The free volume approach of Turnbull and Cohen considered the probability of a sufficient void occurring to accept the molecule. Based on the argument that a successful jump

depends upon both sufficient energy to overcome the potential energy barrier and sufficient void space into which to jump, Macedo and Litovitz (24) combined the two approaches into the hybrid equation

$$\eta = A_o \exp\left(\frac{\Delta H_a}{RT} + \frac{BV_\phi}{V_f}\right) \qquad (26)$$

This expression has been given a theoretical interpretation by Naghizadeh (25); the derivation parallels that of Turnbull and Cohen, but considers the energy associated with the free volume, $\varepsilon(V)$, as a quadratic expression in $(V - V_f)$. Equation (26) has been used successfully to describe the temperature dependence of many low molecular weight liquids.

1.5 Excess Entropy and Enthalpy Theories of the Temperature Dependence of Viscoelastic Behavior

The glass transition displays many characteristics of a second order phase transition, e.g. the thermodynamic state functions, such as the volume V, entropy S, and enthalpy H, are continuous across the transition whereas their derivatives with respect to temperature and pressure, the thermal expansivity α, isothermal compressibility β, and specific heat C_p, are discontinuous. Assuming equilibrium in the liquid and glassy states, the following analogues of the Clapeyron-Clausius equation, known as the Ehrenfest equations, may be derived at the phase transition

$$dT_g/dP = \Delta\beta / \Delta\alpha \tag{27a}$$

$$dT_g/dP = T_g V_g \Delta\alpha/\Delta C_p \tag{27b}$$

where $\Delta\alpha$, $\Delta\beta$, and ΔC_p are the differences in the thermal expansivity, compressibility, and specific heat across the transition. Equation (27a) results from assuming the volume, whereas Eq. (27b) results from assuming the entropy or enthalpy to be continuous across the transition.

Experimentally, Eq. (27a) results in the inequality

$$dT_g/dP < \Delta\beta/\Delta\alpha \tag{28}$$

whereas Eq. (27b) is usually found to hold. Davies and Jones have shown that Eq. (28) would result were it necessary to describe the glassy state in terms of two or more ordering parameters (26); these ordering parameters are additional independent thermodynamic variables introduced to describe the configurational state of the glass (27). However, the equality, Eq. (27b), would still be valid. Based on these results, Goldstein has suggested that either the excess enthalpy or the excess entropy, rather than the free, or excess, volume would better describe the glass transition (28). Substituting an excess enthalpy (28), or an excess entropy (29), in place of the free volume in the Doolittle equation yields the WLF equation with an appropriate redefinition of the parameters c_1^g and

c_2^g in Eq. (23).

Various approaches have been used to describe the glass transition in terms of an excess entropy. The most quantative of these is due to Gibbs and DiMarzio (30) who argue that although the observed transition is a kinetic phenomenon, the underlying mechanism represents a true second order thermodynamic transition; the observed transition T_g is merely an artifact resulting from the impossibility of performing an infinitely slow experiment. Using a quasi-lattice model, and assuming that the vibrational and electronic degrees of freedom do not significantly interact with the external translational and rotational states of the molecule, they calculated the configurational partition function of the polymer system. In an infinitely slow experiment, the equilibrium configurational entropy becomes zero at the theoretical glass transition temperature, T_2.

The gap between the equilibrium theory of Gibbs and DiMarzio and the empirical kinetic approach (WLF equation) was bridged by Adams and Gibbs (31). By calculating the probability that a group of segments reside in a region susceptible to cooperative rearrangement, an expression similar to the WLF equation results in which the constants are interpreted in terms of the entropy. Using experimental heat capacity data, the nearly universal values of these constants were recovered. Since the predictions of the various theories reduce essentially to the same form, it has not been possible to determine their relative merits, nor, in fact, has it been

possible to establish the molecular parameters of the WLF equation. Thus one immediate advantage of including pressure as an additional variable will be a reduction in the number of degrees of freedom for choosing these parameters.

In concluding this section it should be noted that although the entropy based Gibbs-DiMarzio and Adams-Gibbs theories yield added insight into the molecular mechanisms underlying the glass transition phenomenon, they do not preclude the usefulness of the free volume approach. The argument of Goldstein is possibly wrong since it is based upon an inconsistent analysis of the experimental data. Referring to Eqs. (27a) and (27b), let us consider the technique typically used to apply these equations to the experimental results. The value of dT_g/dP is assumed approximately constant and equal to $(T_{g,1} - T_{g,2})/(P_1 - P_2)$, where $T_{g,1}$ and $T_{g,2}$ are the glass transitions at P_1 (usually one bar) and P_2 (typically of the order or 2000 bar) respectively. The quantities in Eq. (27b) are almost invariably measured at atmospheric pressure, P_1, in the area of the glass transition $T_{g,1}$; let us define the parameters so determined as $\Delta\alpha(T_{g,1}, P_1)$ and $\Delta C_p(T_{g,1}, P_1)$. However, $\Delta\beta$ is almost invariably measured at an elevated pressure, $\Delta\beta(T_{g,2}, P_2)$. Experimentally it is usually found that

$$dT_g/dP < \Delta\beta(T_{g,2}, P_2)/\Delta\alpha(T_{g,1}, P_1) \tag{29a}$$

whereas

$$dT_g/dP = T_{g,1} V_{g,1} \Delta\alpha(T_{g,1}, P_1)/\Delta C_p(T_{g,1}, P_1) \qquad (29b)$$

Bridgeman found that both the compressibility and thermal expansivity decrease with increasing pressure; furthermore, the thermal expansivity decreases significantly less than the compressibility (32). Since P_2 is usually greater than P_1 by several thousand bars, it is not too surprising that the inequality (29a) is found rather than the equality (27a); furthermore, the quantities in Eq. (27b) are consistently determined.

This is further substantiated by extensive volumetric measurements carried out by Breuer and Rehage (33) and Quach and Simha (34) on polystyrene. Breuer and Rehage found $\Delta\beta$ vary considerably with both temperature and pressure. However, they had sufficient data over a range of pressure and temperature to extrapolate to atmospheric pressure to achieve $\Delta\beta(T_{g,1}, P_1)$. Comparing the extrapolated value of $\Delta\beta$ with $\Delta\alpha$ resulted in the equality, Eq. (27a). Quach and Simha found similar results on both polystyrene and poly (orthomethylstyrene).

1.6 Time-Pressure Superposition

It has been well established that the viscosity of simple liquids increases with the application of a hydrostatic pressure(32). The free volume approach used for describing the temperature dependence of viscosity is easily extended to the description of the

pressure dependence by defining the free volume as

$$f(P) = f_o - \beta_f(P - P_o) \tag{30}$$

where β_f is the compressibility of the free volume. Combining Eq. (30) with the Doolittle equation, Eq. (19), yields

$$\log a_p = \frac{(B/2.303\ f_o)\ (P - P_o)}{f_o/\beta_f - (P - P_o)} \tag{31}$$

Eq. (31) was proposed by Ferry and Stratton (35). The compressibility of the free volume β_f is assumed to be of the order of $\Delta\beta$. Since the compressibility is quite nonlinear with pressure, this expression should be valid only over a limited range of pressure.

Although the pressure dependence of the compressibility is nonlinear, the bulk modulus, which is simply the reciprocal of the compressibility, depends linearly on pressure for a wide variety of materials, and may be expressed as

$$K(P) = K^* + kP \tag{32}$$

where K^* is the bulk modulus at zero pressure, and k is the slope. If the compressibility is defined as

$$\beta(P) = -\frac{1}{V_o}\left(\frac{\partial V}{\partial P}\right)_T \tag{33}$$

Eq. (32) may be integrated to give

$$(V - V_o)/V_o = \frac{-1}{k} \ln\left(\frac{K^* + kP}{K^* + kP_o}\right) \tag{34}$$

which is known as the Tait equation (36). If the compressibility is defined in the usual sense as

$$\beta(P) = - \frac{1}{V} \left(\frac{\partial V}{\partial P}\right)_T \tag{35}$$

integration of Eq. (32) yields

$$\frac{V}{V_o} = \left(\frac{K^* + kP}{K^* + kP_o}\right)^{-1/k} \tag{36}$$

which is known as the Murnaghan equation (37). Both expressions, (34) and (36), describe the pressure dependence of the volume remarkably well.

Dielectric relaxation measurements (38) performed under constrained bulk compression up to 1,380 atmospheres showed a linear pressure dependence of log a_P. Based on these results O'Reilly (38) assumed

$$f = \frac{f_o + \alpha_f(T - T_g)}{a' + b'P} \tag{37}$$

which, when substituted into the Doolittle equation, yields

$$\log a_{T,P} = \frac{c' f_o P - \alpha_f a' (T - T_g)}{f_o \left[f_o + \alpha_f (T - T_g)\right]} \qquad (38)$$

In Eq. (38), a' and c' are constants, and are not to be confused with the constants, k and K^*, in Eq. (32); Eq. (38) predicts the free volume to be inversely proportional to pressure, whereas Eq. (32) predicts the compressibility to be inversely proportional to the pressure.

The complex bulk modulus (or compliance) of several polymers, including elastomers, has been the subject of several investigations (39, 40). In such measurements, however, pressure is the primary variable corresponding to the shear or tensile stress in measurements of the shear or tensile modulus. We are concerned here with the effect of pressure as a secondary variable, i.e. with the effect of pressure on the (time dependent) shear or tensile modulus. Few investigations have been directed towards studying this effect.

The effect of pressure on the tensile and ultimate behavior of polymers has been studied in a number of investigations; this field has recently been reviewed by Radcliff (41). In general, these investigations have not been concerned with the time dependent properties, but specifically with yield and fracture criteria. Tensile measurements on elastomers by Patterson (42) under superposed hydrostatic pressure clearly established that the effect of increasing pressure on Young's modulus was similar to the effect

of decreasing temperature (c.f. Fig. 1).

Zosel (43) used the torsion pendulum for stress relaxation measurements to study the effect of superposed hydrostatic pressures up to 1,000 atmospheres on the mechanical properties of poly (vinyl chloride). The results did not extend over a wide enough pressure range to decide between Eqs. (31) or (38). It will be shown in Chapter 4 that Zosel's results may be described by the proper application of the Tait equation to the free volume model.

Investigations performed by Jones and Tabor (44) and Billinghurst and Tabor (45) have utilized the torsion pendulum to study the effect of pressure on the isochronal shear modulus and loss tangent (tan δ) of a large variety of polymers, including elastomers. In general, these studies have been too sketchy for any quantitative conclusions.

2. APPARATUS AND EXPERIMENTAL PROCEDURE

This chapter describes the apparatus, procedure, and materials used in the study of the effect of pressure on the viscoelastic response of elastomers.

2.1 Apparatus

Several investigators have used a freely oscillating torsion pendulum to measure an isochronal shear modulus and loss peak (tan δ) up to 1.5 kbar pressure (43-45). There are two major disadvantages to this approach. First, moduli or compliances are functions not only of the frequency but of the damping constant as well. Both frequency and damping depend on apparatus parameters, besides the properties of the specimen. Thus, although the pressure (or temperature) at which tan δ exhibits a peak can be obtained from measurements in free oscillations, the moduli or compliances have at best qualitative meaning only, except at very low damping. Second, utilization of the torsion pendulum at high pressures requires that the viscous damping contributed by the medium be taken into account. None of the investigators reported the magnitude of the viscous forces. Judging from the relative sizes of the pendulum and specimen, they were most probably equivalent, if not greater than, the specimen forces being measured. Zosel (43) also performed stress relaxation measurements in torsion by using the

torsion pendulum in the aperiodic mode. Such measurements defy satisfactory analysis.

Creep and stress relaxation measurements in uniaxial tension have been carried out under superposed hydrostatic pressures up to 2.0 kbar (46). The stress relaxation measurements utilized a spring for extending the specimen to some fixed extension; the subsequent relaxation was then measured with strain gages mounted inside the pressure vessel. The creep measurements were performed by loading the specimen with a weight within the vessel and measuring the subsequent creep with an LVDT. Both measurements were initiated by fusing a wire once the desired pressure and temperature were obtained. The effect of the heat generated in this way on the temperature of the system was not discussed. The measurements were not extensive enough for any quantative analysis of the effect of pressure on the viscoelastic response. In creep measurements, again, viscous forces contributed by the pressurizing medium must be taken into account.

The simplest technique for measuring the intrinsic time dependence of the mechanical properties of materials is stress relaxation in uniaxial tension. No geometric complexities arise since the specimen can easily be made long enough so that end effects may be neglected and a uniform stress field is obtained. Furthermore, once the specimen is extended, no further changes in size or shape occur, thus further simplifying the analysis. These

advantages become particularly attractive when studying the effect of pressure on the material's response. Once the experiment is initiated, the resulting measurements are static; thus viscous forces contributed by the pressurizing medium have no effect on the measurements. The only constraint on the apparatus is that it be versatile enough to measure material properties over about three decades of response, i.e. from rubbery to glassy behavior. Thus the apparatus must accommodate a variety of displacements and forces for exciting the specimen.

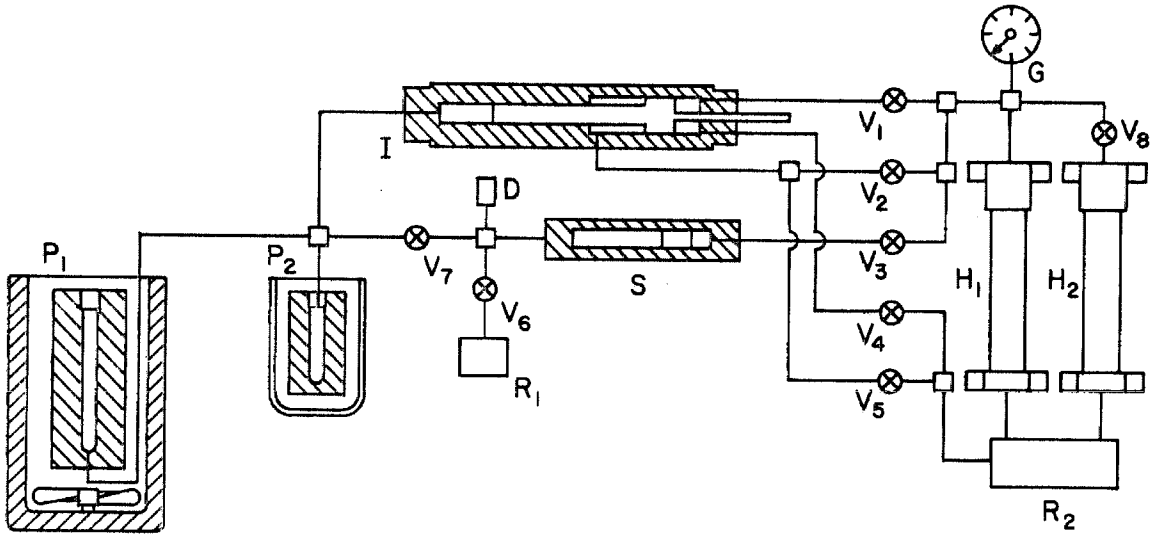

Figure 3. High pressure apparatus ~0 - 5 kbar: D, rupture disk; G, Bourdon gage; H, hand pump; I, 10:1 intensifier; P, high pressure vessel; R, fluid reservoir; S, 1:1 separator; V, two-way valve.

The apparatus designed, constructed and used for the stress relaxation measurements is shown diagrammatically in Fig. 3. The heart of the system is the stress relaxometer; its function is to impose a step function of strain to the specimen and measure the resulting stress decay as a function of time. The hydrostatic environment is obtained by placing the relaxometer in a suitable pressure vessel. The remainder of the system comprises the necessary equipment for the generation and measurement of the required temperatures and pressures.

2.11 Stress Relaxometer

The relaxometer, Fig. 4b and Appendix A, was fabricated by the Chemical Engineering Machine Shop. The specimen is held between two spring-loaded concentric cylinders (I and O). A removable snap-ring (SR) allows springs of various stiffness to be inserted between the cylinders, depending upon the force required. A small hole (H) drilled through the U-shaped copper strips cemented to the ends of the specimen (E) allows the specimen to be attached to the removable end cap (C). The specimen is then lowered into the cylinders and attached to the bottom clevis (G) with a screw-pin; clearance holes through the outer and inner cylinder allow easy insertion of the pin. The bottom clevis assembly is attached to the outer cylinder via a dowel pin (P). The inner cylinder is slotted for this pin, thus allowing vertical travel without

rotation. Pre-stressing the spring (S) forces the two cylinders apart until the bottom cap engages the dowel pin; spacers of various thickness may be inserted in this space to change the amount of travel, and, consequently, the displacement of the specimen. When the two cylinders are pressed together, a hook machined on the bottom cap engages the latch (L). The latch is shaped such that the mechanism is triggered when the solenoid (D) is activated. In practice, the proper combination of spring and spacer is chosen so that the energy of the compressed spring is greater than the energy required to extend the specimen. When this condition is satisfied, the cylinders are extended until the bottom cap of the inner cylinder engages the dowel pin. The specimen is extended simultaneously and held fixed throughout the experiment. The resulting force decay or relaxation of the specimen is then measured via the strain gages incorporated in the lower clevis assembly.

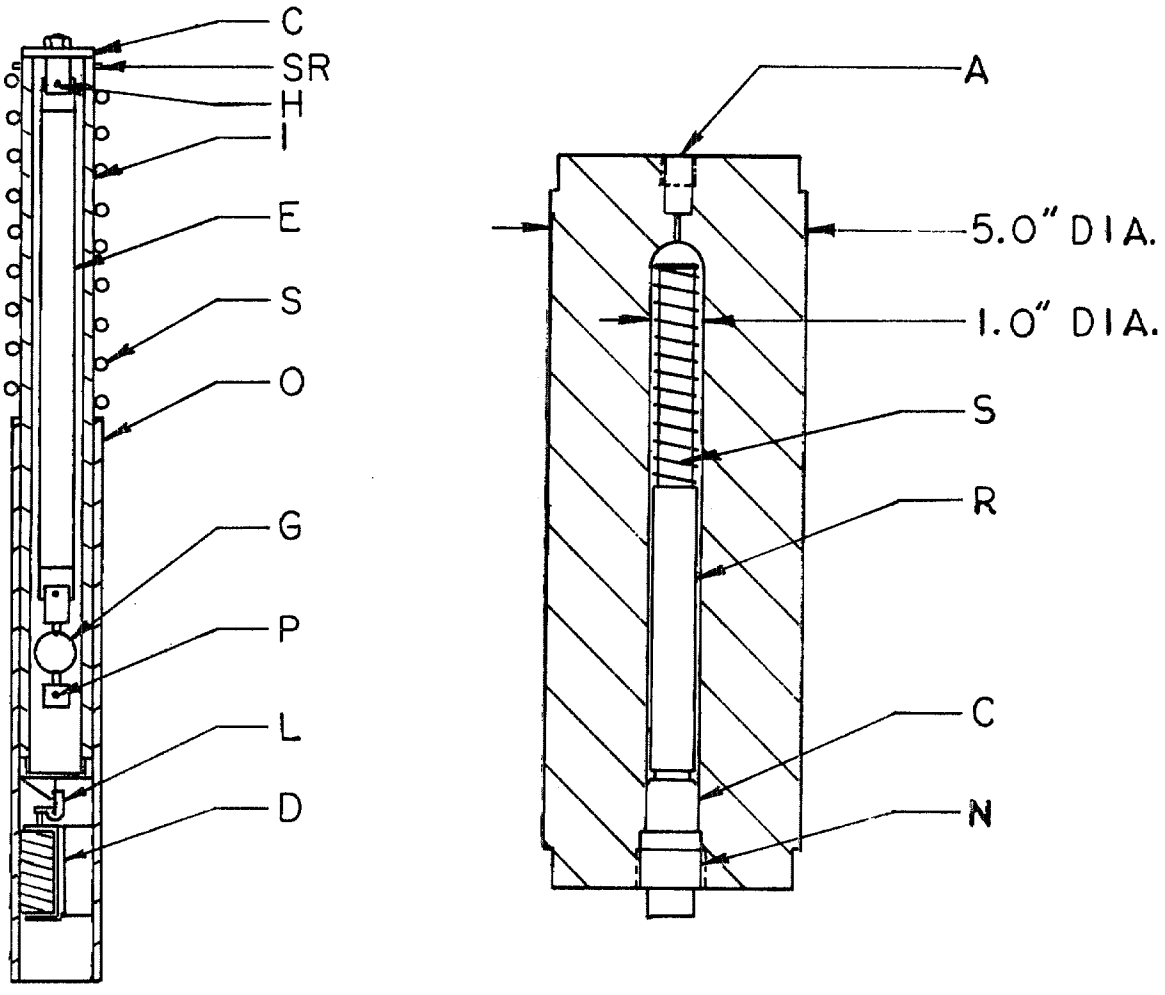

Figure 4. Stress relaxometer (a) and pressure vessel (b): A, AE cone connection; C, end cap; CP, closure plug; D, solenoid; E, specimen; G, strain gage assembly; H, attach hole; I, inner cylinder; L, latch; N, nut; O, outer cylinder; P, dowel pin; R, relaxometer; S, spring; and SR, snap-ring.

Considerable difficulties were encountered with the triggering mechanism. As the experimental pressures become higher, so does the response of the specimen, since the glassy state is being

approached. Thus a stiffer spring is desired in order to extend the specimen. A stiffer spring requires a stronger impulse from the solenoid in order to trigger the mechanism. The Electromechanisms SP-37 solenoid consists of a steel rod which slides in a nylon tube around which the coils are wound; this rod is both guided and pulled by a steel bushing when the coil is energized. Thus, in order for the rod to move, it must overcome the viscous resistance of the pressure generating fluid between the nylon tube and the rod, and displace the fluid in its path. Both displacements become more difficult as the viscosity increases due to higher operating pressures. Thus the mechanism becomes progressively more difficult to activate with increasing pressures. For successful operation at the higher pressures the latch had to be carefully set so that the slightest jar would trigger it. This practice requires repeated attempts at inserting the relaxometer in the pressure vessel without triggering the mechanism. Furthermore, when the desired pressure and equilibrium is obtained, sometimes the solenoid will not fire the mechanism. The system must then be depressurized, dismantled, and reloaded.

Two J. P. Semiconductors (JP 090 120) strain gages are mounted on the stainless steel ring incorporated in the lower clevis assembly. The half-bridge circuit minimizes the effects of pressure and temperature on the calibration of the gages. The two gages are mounted on the inner and outer diameters of the ring to

minimize nonlinearity of the output of the gages. Subsequent calibration of the gages (see 2.17) showed the output voltage of the bridge circuit to be linear with force; although both pressure and temperature shifted the zero of the bridge, only temperature affected the response of the gages.

Considerable difficulties were encountered in obtaining success with this arrangement. The first and second strain gage assemblies had excessive cement between the semiconductor gage and the stainless steel ring; calibration of the gages showed unacceptable hysteresis due to relaxation of the epoxy bonding agent. This problem was solved by minimizing the amount of cement. The third and fourth assemblies failed at elevated pressures due to cracking of the gage mounted on the inner diameter of the ring. This was found to result from the high pressure compressing the cement and forcing the relative brittle, flat gage to assume the circular configuration of the ring. The problem was solved by flattening the ring in the area where the gages were mounted. The fifth assembly failed due to a faulty gage. The sixth attempt was successful and no further problems have occurred. The first three assemblies were made by the Chemical Engineering Machine Shop; the latter assemblies were accomplished by J. P. Semiconductors.

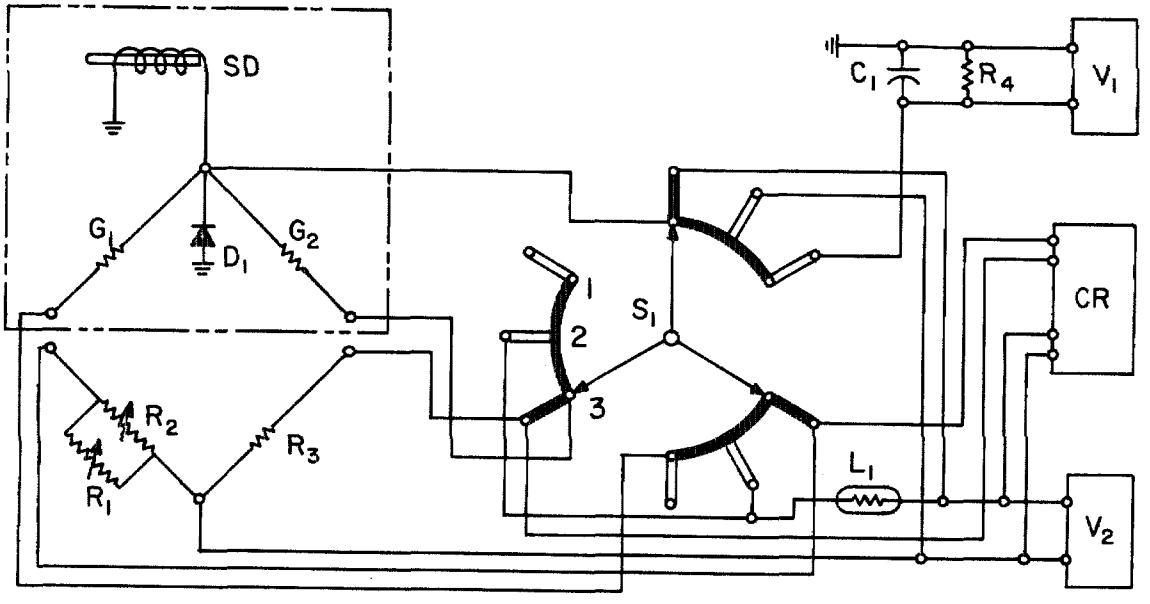

Figure 5. Electrical Circuit for Stress Relaxometer: C, capacitor; CR, strip chart recorder; D, diode; G, strain gage; L, safety light; R, resistor; S, switch; SD, solenoid; and V, voltage supply.

The electrical circuitry for measuring the output of the strain gages and for firing the solenoid is shown in Fig. 5. The solenoid (SD) is fired through a 10,000 μfd capacitor (C_1) in parallel with a 250 ohm resistance (R_4) from a Hewlett-Packard Model 6218A voltage supply (V_1). The 40 V silicone diode (D_1) protects the strain gages against inductive feedback from the solenoid. The strain gages (G_1 and G_2) form a half-bridge compensated by another half-bridge consisting of a 100 ohm precision resistor (R_3), and two ten-turn helipots (R_1 and R_2) in parallel. The output from the strain gages is recorded on a Hewlett-Packard Model 7100 BM two-pen

strip chart recorded (CR); the second pen is used either to monitor the voltage across the bridge or to measure the output of a thermocouple placed in the temperature bath. Since electrical leads into the high pressure vessel are at a premium, the common lead to the strain gages is also used to fire the solenoid to ground. A three-way switch is used so that the remaining two leads for the strain gages may be opened (Position 1) when firing the solenoid. The electrical leads in the bottom plug of the pressure vessel periodically short out due to pressure cycling; this causes the 40 volts used to fire the solenoid to be put across the strain gage having the shorted lead, which ruins the gage. Thus the center position (2) of the three-way switch is a test position for shorts.

2.12 Pressure Vessels

Two pressure vessels are incorporated into the system, the larger of these, Fig. 4b, houses the stress relaxometer. It consists of a 16 inch long beryllium copper cylinder of 5 inch outer and one inch inner diameter. The relaxometer (R) is held in position by the closure plug (CP) which in turn is secured by the stainless steel nut (N). The smaller vessel, an 8 inch long beryllium copper cylinder by 2.5 inch outer diameter, houses the coil of manganin wire used for measuring the pressure in the high pressure portion of the system. Both vessels were fabricated by the Chemical Engineering Machine Shop and subsequently heat treated

at 600°F per hour per inch of material. After approximately 100 pressurizations in the neighborhood of 5 kbar, the sealing area of the inner diameter was found to have expanded in both vessels to the extent that an adequate seal was no longer possible. Thus, the sealing areas were remachined and new bottom closure plugs and bevel rings made. Both vessels use the AE-Cone connection by Autoclave engineering for connecting the high pressure line to the vessel, as indicated in Fig. 4b.

2.13 Closure Plug

The bottom closure plug (see Fig. 6) serves as a base for the relaxometer and contains the three electrical leads (L) for the strain gages and the solenoid. The pressure seal is due to Warschauer and Paul (47). A standard O-ring (O) makes the initial seal. Expansion of the beveled ring (B) with increasing pressure forms a seal at the higher pressures. The plug, ring and the three cones (C, only one is shown in the figure) are made of beryllium copper and heat treated at 600°F for one hour.

The plug is assembled by first soft soldering #22 AWG stranded wire leads to the bottom of the cones. The leads are then soldered to the tips of the cones, and all flux is removed with acetone. The leads are straightened until the cone falls naturally in place when inserted into the closure plug. The cone is removed and a small amount of epoxy is applied around the tip of the cone.

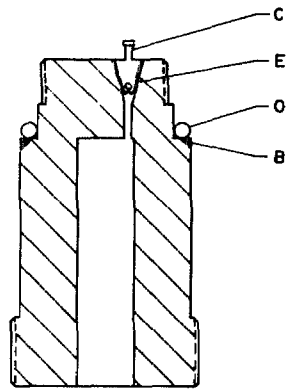

Figure 6. Bottom Closure Plug: B, beveled ring; C, cone; E, epoxy seal; and O, O-ring.

The cone is now "gently" pulled into place with a slight rotation to distribute the epoxy uniformly. Seating the cone too deeply results in a short circuit; too much epoxy causes premature failure by cracking of the epoxy. These seals were found to endure approximately 40 pressurizations to 3 kbar before replacement was necessary.

The cones are removed by placing a hot soldering iron on the base until they can be pulled out. Since this procedure destroys the other two leads as well, all three must be replaced together. The epoxy adhering to the cone may then be removed with a razor blade

using extreme care not to scratch the cone. The epoxy remaining in the plug is drilled out; that remaining in the conical section of the plug may be removed with an Exacto knife, again using extreme caution not to scratch the beryllium copper. The components are then soaked in benzene and reassembled. It was found that after rebuilding the plug several times, the epoxy became fairly easy to remove because residual silicone oil acted as a release agent.

2.14 Manganin Coil

The 64 ohm manganin coil was non-inductively wound by hand, and seasoned according to Babbs (48) by alternatingly baking the coil at 140°C for 8 hours and soaking it in dry ice at -80°C for several hours; this process was continued for several days. The coil is then cycled from atmospheric to the highest pressure used until the resistance at one atmosphere stablizes. The coil rests on the bottom closure plug of the smaller pressure vessel. This plug is a scaled-down version of the larger plug, except that it has but one electrical lead. The resistance of the coil is measured with a Leeds-Northrup Model 8067 Mueller Bridge and a Leeds-Northrup Model 2430-C Galvanometer. The resistance-pressure coefficient of the coil was measured to be 6506.3 ohms/bar as described in Section 2.17.

2.15 Pressure Generating System

Pressure is generated using two hand pumps, a 10:1 intensifier, a 1:1 separator, and the necessary valves, lines, and fittings for their connection. The two Enerpac handpumps are connected in parallel such that the low pressure-high capacity (10,000 psi-0.43 cubic-inch per stroke) rough pump may be utilized for the initial compression stages; this is the range in which most of the volume contraction occurs due to both initially high compressibilities of the fluids and entrapped air. The high pressure-low capacity (40,000 psi-0.043 cubic inch per stroke) pump is then used for the final compression. A Bourdon tube gage is used to monitor the pressure on the low pressure side of the system. A one gallon plexiglass reservoir insures an adequate supply of hydraulic fluid for the pumps.

The 10:1 intensifier was purchased from Autoclave Engineers. A piston ratio of 10:1 yields a pressure boost of approximately 9:1 after frictional losses are accounted for. Since the stroke of the intensifier is only 5 inches, it is necessary to prime the high pressure side of the system to approximately 5,000 psi before using the intensifier.

The 1:1 separator allows the system to be primed without contaminating the silicone oil used in the high pressure side of the system with the hydraulic fluid used in the low pressure side. The separator was fabricated by the Chemical Engineering Machine Shop.

All valves, tees, burst disks and the tubing were purchased from Autoclave Engineers, Inc. All tubing joints incorporate Autoclave AE-Cone connections.

2.16 Temperature Control

The temperature of the relaxometer is controlled by completely immersing the inverted pressure vessel in a continuously stirred bath (49). A Hallikainen 1053-B Thermotrol is used in conjunction with a platinum resistance thermometer for sensing, and a nichrome wire loop for heating the silicone oil bath. Excess heat is removed by tap water, ice water, or liquid nitrogen when controlling at or above 25°C, 15°C, or -30°C respectively. A secondary resorvoir is used for raising and lowering the fluid level of the bath when removing the relaxometer for specimen loading.

The hole through the bottom plug of the inverted pressure vessel serves as a well for a mercury thermometer capable of being read within ±.01°C. An iron-constantan differential thermocouple is used for temperature measurements below 0°C. The second pen of the strip chart recorder may be used for measuring the voltage across the thermocouples; generally, however, this pen is used to monitor the voltage across the strain gage bridge. The temperature of the bath was found to be controllable within ±.02°C throughout an experiment.

To monitor the temperature lag between the bath and the

interior of the pressure vessel and to determine the effect of firing the solenoid, a calibrated platinum wire was placed across two of the three electrical leads. Approximately 20 minutes were required for the interior of the vessel to reach the temperature of the bath after a 5°C temperature increment; no temperature rise was found when firing the solenoid. In practice, both temperature and pressure affected the zero of the strain gage bridge circuit; thus it was easy to determine when equilibrium was obtained by monitoring the zero of the bridge.

The vessel containing the manganin coil was originally intended to operate in the open at room temperature. However, under these circumstances several hours were required for equilibrium to be reached after the adiabatic temperature rise following compression. The problem was solved by immersing the vessel in a Dewar flask at 0°C. Approximately 20 minutes were required for equilibrium once installed in the bath.

2.17 Calibration

The following procedures were used to calibrate the extension of the relaxometer for measuring the strain imposed on the specimen, the voltage-force coefficient of the strain gages used to measure the stress relaxation of the specimen, the resistance-pressure coefficient to the manganin coil for measuring the pressure of the system, and the effect of temperature and pressure on the

various calibrations. The extension of the relaxometer when triggered was measured with a 0 - 1.0 inch dial indicator capable of measuring within 0.0002 inch. The relaxometer was clamped in a vice and the dial indicator placed over it using a height stand. The extensions resulting from inserting the various spacers in the relaxometer were measured. The spacers were then marked to insure that they would always be used in the same orientation.

The strain gages were calibrated by simply hanging known weights from the clevis portion of the strain gage assembly; the response was found to be linear from 0 to 8 pounds. No measurable change in the length of the strain gage assembly was detected with the 8 lb. load. In practice, the voltage across the bridge (approximately 1.5 volts) is adjusted so that 5.00 millivolts are measured with a 1.0 pound weight.

The effect of temperature and pressure on the strain gages was determined by loading a light spring (about 1.0 lb. when extended 0.5 inch) in the relaxometer in place of a specimen. The system was then pressurized to various pressures (or brought to various temperatures) and the relaxometer was triggered. Since temperature and pressure have negligible effects on the spring's modulus, the difference in output may be attributed to the strain gages. Pressure had no effect on the output of the gages, although the zero was shifted. Temperature shifted the response of the gages by 2.43×10^{-3} lbs/^{o}C in a linear fashion.

The resistance-pressure coefficient of manganin wire is linear up to approximately 12 kbar. Unfortunately the actual value of this coefficient varies considerably from batch to batch; in fact coils wound from the same spool may vary (48). It is therefore necessary to calibrate each coil. A single point calibration at the freezing point of mercury (7,565 bar at 0^{o}C) is reported to allow pressure measurements within 0.5% to be made (48). Thus, both the resistance and the voltage drop across a mercury reservoir were measured as a function of pressure. Although both methods detected the transition, it was not sharp enough to assign a specific value to it. The smeared transition was probably due to contamination of the mercury, perhaps by the silicone oil. Mercury is very undesirable around solder joints. About four attempts all resulted in mercury contamination of the solder joints of the bottom closure plug. Since these joints may not be resoldered without ruining the epoxy seals, the entire plug had to be rebuilt each time.

The calibration was finally made with a Heiss Bourdon tube gage. The coil was calibrated at 10,000, 20,000, and 25,000 psi within 0.1%. The calibration was linear with pressure up to 25,000 psi and was extrapolated to the higher pressures. Since the coil was always used at 0^{o}C, it was not necessary to determine the effect of temperature on the calibration.

2.2 Experimental Procedure

The experimental procedures described below were developed in the course of the measurements. This probably explains why the last material studied, Hypalon, showed the least experimental error. Various improvements in technique may still be made, and suggestions are given where problem areas persist.

The experimental procedure consists of ten basic steps: (1) specimen preparation; (2) loading the specimen; (3) loading the relaxometer into the pressure vessel; (4) pressurizing the system; (5) obtaining the desired temperature; (6) achieving specimen equilibrium; (7) triggering the mechanism; (8) recording the relaxation of the specimen; (9) depressurization; and (10) specimen removal. The specimens were cut to size (0.080 x 0.080-0.375 x 4.4 inches) by the Chemical Engineering Machine Shop from 0.080 inch thick rubber sheets. The copper end clips were then bonded to the ends of the specimens to yield approximately 4.5 inches between holes. In order to achieve a satisfactory bond between the copper clips and the rubber specimen, the copper clips were cleaned in dilute HCl, rinsed with distilled water, and dried. The specimen was lightly buffed with a wire wheel in the area to be bonded; this area was then wiped clean with acetone and allowed to dry. A quick drying cement (Eastman 910 or Zip-Grip 10) was lightly applied to the specimen and allowed to set for about one minute. This allows the cement to absorb moisture from the air. The copper clip was

then held with a pair of pliers, and the specimen was quickly slipped into place and aligned. The copper clip was then gently squeezed to the specimen for one minute. Too much pressure will squash the specimen. Too little pressure results in a poor bond. Once a copper clip or specimen has been exposed to the silicone oil no further attempts at bonding should be made. Also, bonding should be carried out in an area removed from the apparatus, with separate tools, and care must be taken not to expose one's hands to the silicone oil. In general, specimen preparation should not be taken lightly; considerable time can be wasted in inserting a poorly bonded specimen into the pressure vessel, pressurizing the system, waiting for equilibrium, and having the bond fail when the specimen is extended. When this happens, the removable end cap may be retrieved from the bottom of the pressure vessel, using considerable patience, with a piece of brazing rod having a right-angle hook at one end.

Once the strain gages are calibrated (see Section 2.17) the specimen may be loaded into the relaxometer. Selecting a specimen of proper width and a spacer of proper thickness requires some experience. The maximum permissible force is about five pounds; stronger springs may be used, but triggering becomes difficult. Recording forces less than about 0.2 pounds resulted in considerable error; this may have been due in part to using the 2.0 millivolt scale on the recorder which tended to have considerable drift.

Additionally, overextending the specimen will result in a nonlinear response of the specimen. In general, the experiments at one atmosphere may be run with a 0.375 inch wide specimen and maximum displacement; linearity should then be verified by duplicating the test with a smaller displacement. Experiments at higher pressures are then conducted using decreasingly smaller specimens and displacements. The region of linear response also decreases as the glass transition is approached, therefore making it necessary to continually verifying linearity.

Assuming a specimen and spacer of the proper size have been chosen, the specimen is loaded in the following manner. The relaxometer is latched in the down position, and the spacer is put in place. The specimen is inserted in the clevis of the removable end cap, and the screw-pin is put in place. The relaxometer is then held upright while the specimen is lowered into position and secured with the other screw-pin. The relaxometer is then inverted and the nut on the end cap is adjusted to remove the slack from the connection; the recording pen is used to detect this point. Once the O-ring and the beryllium copper bevel ring are straightened, the relaxometer is ready to be inserted into the pressure vessel.

The relaxometer is lowered into the pressure vessel until the O-ring comes in contact with the sealing diameter of the inner bore. Valve V_6 is opened to allow the silicone oil in the pressure vessel to be transferred back into the filling reservoir. The relaxometer

is then pushed firmly into the pressure vessel, and the stainless steel nut screwed into place. Throughout the loading operation, the output of the strain gages should be monitored; a sharp jump usually indicates accidental triggering of the mechanism. This is especially critical when the experiment to be run is to be in the glassy or transition region since both the specimen size and extension will be small, resulting in a very small response at atmospheric pressure.

The triggering mechanism rarely fired prematurely after the system was primed to approximately 5,000 psi through the 1:1 separator. Furthermore, a metallic click could usually be detected if there was little background noise in the room. Thus, initial pressurization should always precede preparation of the temperature bath, since the impeller motor makes considerable noise. Once primed, valve V_7 is closed, valve V_1 opened, valve V_3 closed, and valve V_6 opened respectively; it is important that valve V_6 be opened throughout the experiment since any leakage occuring in valve V_7 will introduce high pressures into the 1:1 separator. The low pressure side of the system is then pressurized to 5,000 psi with the rough pump, P_2, using the Bourdon tube gage to estimate the pressure in the high pressure side of the system. When the desired pressure is approached, pump P_1 is used in conjunction with the manganin coil to obtain the final pressure. The pressure will continue to drop until equilibrium is established from the adiabatic

heating, or due to leaks in the system. Leaks usually result from either bad electrical leads of bad O-rings. Since both kinds of leak show drips from the bottom nut of the corresponding vessel, they can not be distinguished from one another. If replacing the O-ring does not stop the leak, the electrical leads should be rebuilt.

Operating the temperature bath at 25°C requires a coolant to remove the excess heat formed in circulating the silicone oil bath; it also reduces the thermal lag of the system and allows the Hallikainen Thermotrol to operate more smoothly. Circulating tap water through the cooling coils of the temperature bath provided adequate cooling in the winter months. For operation in the summertime, it was necessary to cool the tap water with ice; this was accomplished by placing additional cooling coils in a Coleman ice chest. For operation at lower temperatures, liquid nitrogen is circulated through the cooling coils. The lowest temperature obtainable with the ice chest arrangement was about 16°C. This took about four hours due to the thermal inertia of the bath.

The temperature is measured by placing a mercury thermometer in the bottom nut of the pressure vessel. When operating the bath below 0°C, the differential iron-constantan thermocouple is used in conjunction with the chart pen normally used to monitor the input voltage to the strain gage bridge circuit. This allows the top of the bath to be covered. Also the nitrogen exhaust may be circulated over the surface of the bath. This decreases the amount

of ice formed when removing the relaxometer for specimen loading. The tygon tubing used for circulating the nitrogen is placed down into the pressure vessel to prevent ice formation in the bore.

Temperature and pressure equilibrium is generally obtained long before specimen equilibrium. Since increasing the pressure, or decreasing the temperature, shortens the specimen due to volumetric contraction, the specimen is strained from its equilibrium position when pressurizing the system, or lowering the temperature. Time must be allowed for this stress to relax to a negligible level relative to the stress relaxation to be measured; otherwise the stress relaxation measured in the experiment will correspond to the superposition of two strains, one of unknown magnitude and history. This effect is especially troublesome in the transition region where considerable time is required for this relaxation to reach a negligible level.

Elastomers in the glassy or transition region are highly history dependent. This results in different glasses being formed depending upon the rate of pressurization and the magnitude of the stresses induced through volumetric contraction at constant extension. This effect possibly explains the errors in modulus obtained in the glassy region. Should this be the source of the error, the following improvement in technique could be made. The adjustment screw in the end cap could be used to compensate for the expected contraction predicted form compressibility data.

It would further be necessary to firmly attach the end cap to the relaxometer, and slot the holes in the copper clips used to hold the specimen; otherwise the specimen would be in a curved configuration prior to obtaining the final pressure. This would allow the specimen to remain in a stress free state until the final pressurewas obtained. The major drawback to this approach is that monitoring the system for premature triggering of the relaxometer during loading and pressurization is no longer possible.

Once the relaxation has reached a suitable level, the actual experiment may be performed. The bridge is zeroed, using potentiometers R_1 and R_2, and the proper voltage attenuation (5.0 to 40 mv) of the strip chart recorder is selected. The possibility of short circuits in the electrical leads is checked with the middle position of the three-pole switch; if a short exists, the electrical leads must be rebuilt before performing the experiment since the 40 volts used to fire the solenoid will be put across the strain gage. If there is no short the capacitor is charged, the chart speed set to around 30 cm per minute, and the mechanism is triggered. The switch is immediately turned back to the gage position. One of five responses may be recorded: (1) nothing; (2) the pen will go off scale in the negative direction; (3) the pen will go off scale in the positive direction; (4) the pen will rise to some value, remain fairly constant for some period, and then begin recording a relaxation curve; or (5) the pen will immediately trace out a force

relaxation curve. No response indicates that the mechanism failed to trigger. This is quite common at pressures above 3.5 kbar. If about 20 more attempts still result in failure, the relaxometer should be removed and the latch reset. The pen going off scale in the negative direction indicates that the copper specimen clips have come unbonded. The pen going off scale in the positive direction results, obviously, from the choice of a too sensitive scale. Should the pen record a fairly constant voltage for some period and then suddenly begin relaxing, the specimen has been given too much displacement. Measurements well in the glassy region will yield a similar response, but there will be no sudden relaxation. If a flat spot occurs, the experiment should be discarded and rerun with either a thinner specimen or a smaller displacement. The reason for discarding this type of an experiment is discussed in Section 3.1. If everything goes correctly, a smooth force relaxation curve will be recorded. More sensitive scales should be selected as the relaxation proceeds, and a slower chart speed when the relaxation slows down. The 1.0 and 2.0 mv scales should be avoided since they tend to drift. The best results were obtained when the specimen size and displacement were such that at least 0.5 pound force was being recorded towards the end of the experiment, i.e. after about 20 minutes.

Depressurizing the system is accomplished by first making sure the galvanometer button on the Mueller bridge used for measuring the pressure is up. Valve V_2 is slowly opened and the

pressure released at a rate of about 2000 psi per minute in the low pressure side of the system. Valve V_6 is shut, and valves V_7 and V_3 are opened. The temperature controller and circulating pump are turned off, and the bath level is lowered.

Valve V_6 is opened and air pressure is applied to reservoir R_1 in order to fill the 1:1 separator. After removing the bottom nut of the pressure vessel, valves V_1, V_2, and V_6 are shut, and valve V_7 is opened. The relaxometer is then pumped out of the pressure vessel with pump H_2. Once the relaxometer is completely out of the pressure vessel, valve V_6 is shut to prevent silicone oil in the reservoir from draining back into the pressure vessel. The system is then ready to be reloaded.

2.3 Pressure Medium

The apparatus was originally designed to be operated at pressures up to approximately 7.0 kbar, since most of the "standard" elastomers, such as natural rubber (NR) and styrene-butadiene-rubber (SBR), undergo the glass transition at around 5.0 kbar pressure at room temperature. Several fluids were considered before choosing the Dow Corning 5.0 centistoke 200 Silicone fluid. The more important properties influencing this choice were freezing point, viscosity, electric conductivity, and incompatibility with the elastomers being studied.

Silicone fluids were the first choice since they are available

in a wide range of viscosities, their viscosity is relatively insensitive to temperature and pressure, they have a very low electrical conductivity, and they do not readily interact with hydrocarbons. Several experiments were performed to test whether the natural rubber would swell at the anticipated pressures. If swelling occurred, the relaxation processes would be affected.

Specimens of natural rubber were prepared by crossinking with 3 parts of dicumyl peroxide at 250°F for 20 minutes at 25,000 psi. The 0.080 inch thick sheet was cut into 0.05 x 6.0 inch strips, and quickly dipped in silicone oil, wiped, and weighed on the analytical balance. The specimens were then pressurized to 7.0 kbar, quickly removed, wiped in the same manner, and reweighed. No statistically significant difference could be detected within the experimental error. Since these experiments yielded considerable scatter due to the inherent inconsistencies in the wiping operation, further tests were made.

From a similar sheet of natural rubber 0.080 x 0.38 x 6.0 inch strips were cut, and subjected to stress relaxation measurements in the Instron tensile tester over the temperature range from -55 to -60°C. This temperature range is about midway in the transition from rubberlike to glasslike behavior for NR. It is therefore the temperature region in which any change in relaxation behavior should be most easily detected. After the measurements were taken, the specimens were pressurized to 7.0 kbar pressure

for 4 hours, quickly removed, and retested in the Instron. No change in relaxation behavior was detected. It was concluded that swelling of natural rubber by the silicone oil was not a problem, and attention was focused on the possibility of the pressure medium becoming highly viscous at the higher pressures.

Ideally, stress relaxation experiments are initiated with a step function, although in reality one must settle for a relatively sharp ramp function. Assuming a fairly simple viscoelastic model, it is shown in Section 3.1 that approximately 25 times the period of the ramp function is equivalent to that of a step function. Since it is desirable to measure at least three decades of response in a stress relaxation test, it is necessary to extend the specimen as quickly as possible. Otherwise, the total time required for an experiment becomes prohibitive.

The first series of experiments performed with the relaxometer incorporated a light spring in place of a rubber specimen for calibrating the strain gages as a function of pressure up to 6 kbar. After several weeks of perfecting the trigger mechanism, a successful firing resulted at 6 kbar pressure. Approximately one minute was required for the relaxometer to extend 0.5 inch. The problem was attributed to the relatively high viscosity (100 centistoke) of the silicone fluid being used at that time. To correct the problem, a series of lighter grades of Dow Corning 200 silicone fluid were ordered.

The 1 c.s. silicone fluid had a relatively high vapor pressure and also tended to leak quite readily. The 5 c.s. fluid proved to be the lightest fluid which was still easy to handle, and was thus chosen for all subsequent experiments. With this fluid, the relaxometer was always fully extended in the short time required to switch from the S_1 to S_3 position. After performing experiments at the highest pressure on a particular elastomer, the specimen was quickly removed from the pressure vessel and measured with a micrometer; no change in specimen size was ever found with the materials used.

2.4 Materials

The materials originally selected for this investigation were natural rubber (NR) and styrene butadiene rubber (SBR). Unfortunately, the stress relaxometer failed to trigger properly at the 6 kbar pressure necessary for obtaining glassy behavior at room temperature with these rubbers. Since poly (ethylene-propylene-diene-monomer), or EPDM, has a higher T_g (-50°C for EPDM compared to about -70°C for NR and SBR), it was hoped that in this material glassy behavior could be induced with 5 kbar pressure. The results of these measurements are given in Appendix B. The transition region was not reached with the 5 kbar pressure, nor was it possible to apply time-temperature of time-pressure superposition to the relaxation data obtained. Lack of time-temperature superposition in EPDM has been noted previously and has been attributed to both crystallization

(50) and blockiness.

Patterson (42) reported the glass transition in Viton* and Neoprene* to occur around 2 and 3 kbar respectively, at room temperature. E. I. du Pont de Nemours and Co. graciously supplied molded sheets of these two materials together with a sheet of Hypalon*. The compounding recipes of these materials are discussed by Stevenson (52), and are given below in parts per hundred parts of rubber.

Hypalon-40	100
AC, PE 617A	5
SRF Black	4
Epon 828	15
MBTS	0.5
Tetrone A	1.5
DOTG	0.25
Cure: 30 min. at 307°F	

Viton-B	100
M_gO	15
MT Black	20
LD-214	3
Cure: 30 min. at 300°F 1 hr at 212 1 hr 250 1 hr 300 1 hr 350 24 hr 400	

Neoprene WB	50
Neoprene WRT	50
Neozone A	2
Stearic Acid	0.5
MT Black	100
Hard Clay	25
L P O	12
Red Lead	20
Thionex	1
Sulfur	1
Cure: 20 min. at 307°F	

*Trademark of E. I. duPont de Nemours and Co., Inc.

Hypalon-40 is a chlorosulfonated polyethylene containing approximately 30 to 40% chlorine and 1.0 to 1.5% sulfur. This implies approximately 20 chlorine atoms and 1 sulfonyl group for every 100 carbon atoms. AC, PE 617A is a polyethylene added as a lubricant or mold release. SRF Black is a semi-reinforcing furnace black. It has been found to have no effect on the relaxation processes for strains less than 150% (51). The Epon 828 (epichlorohydrin-bisphenol A), MBTS (benzothiazyl disulfide), Tetrone A (dipentamethylene thiuram tetrasulfide), and DOTG (di-o-tolylguanidine) constitute the curing system.

Viton-B is a copolymer of vinylidene fluoride and hexafluoropropylene having the typical polymer segment

$$-CH_2-CF_2-CH_2-CF_2-CH_2-CF_2-CF_2-\underset{\displaystyle CF_3}{\underset{|}{CF}}-$$

The compounding recipe contains medium thermal (MT) carbon black, magnesium oxide, and a diamine curing system (LD-214).

Neoprene (polychloroprene) is manufactured by polymerizing 2-chlorobutadiene to yield a polymer containing approximately 98% monomer units which have added in the 1, 4-position, and 1.5% in the 1, 2-position (52). Cross linking is believed to result mainly from the 1.5% monomer units which add in the 1, 2-positions. Many types of Neoprene are available differing essentially in the curing systems employed. The compounding recipe for the specimens used contain Neoprene WB (noted for its processibility) and Neoprene WRT (noted

for its resistance to crystallization). The stearic acid and LPO (light processing oil) are processing lubricants. The Neozone A (a naphthylamine) serves as an antiozonant. The MT carbon black and the hard clay are reinforcing fillers. The Red Lead (Pb_3O_4), Thionex (tetrabutyl thiuram monosulfide), and sulfur make up the curing system.

3. EXPERIMENTAL RESULTS

The experimental objective was to measure the effect of temperature and pressure on stress relaxation in elastomers, and to determine whether the effect of time, temperature, and pressure would superpose. The major assumption made in a stress relaxation experiment is that material response to a quick ramp function is indistinguishable from a true step function after an appropriate lag time; the validity of this assumption is discussed in Section 3.1.

The material parameter measured in uniaxial tension is the time-dependent Young's modulus, E(t), which is a combination of K(t) and G(t), the time-dependent bulk and shear moduli related to time-dependent changes in size and shape, respectively. Both K(t) and G(t) depend on pressure as well as temperature. It will be shown in Section 3.2 that proper evaluation of the superposition of time, pressure, and temperature effects requires conversion of E(t) to G(t), or additional information on E(t). The difficulties connected with this conversion will also be discussed in Section 3.2.

Section 3.3 presents the experimental data reduced in terms of the shear modulus. These data are then empirically shifted along the logarithmic time axis into superposition to obtain master curves.

3.1 Viscoelastic Response to a Step Function of Strain

In this section we examine the consequences of using a ramp

excitation instead of a step function. We first consider the ideal shear stress relaxation experiment in which a step function of strain is imposed on the specimen at time t = 0. We express the strain excitation as

$$\varepsilon(t) = \varepsilon_o h(t) = \begin{cases} 0 \text{ for } t < 0 \\ \varepsilon_o \text{ for } t \geq 0 \end{cases} \tag{39}$$

where h(t) is the unit step function. Substitution into Eq. (1) yields

$$\sigma(t)/\varepsilon_o = \int_o^t Q(u)\, du \equiv G(t) \tag{40}$$

The shear relaxation modulus, G(t), is seen to be the response to a step function of strain.

Experimentally, the step function must be approximated by a ramp function of rise time t_1 as shown in Fig. 7c. The stress relaxation following a ramp function of strain is usually assumed to be within 1% of the ideal response given in Eq. (40) after a period, or lag time, of $25t_1$ has elapsed. Intuitively, this lag time should be strongly dependent upon the relaxation processes occurring in the polymer. The lag time should be maximum in the transition region where the relaxation processes are of the time scale of the observation, and decay to zero in both the glassy and rubbery regions. In the glassy region any relaxation process is very slow. In the

rubbery region the relaxational processes are very fast compared to the observation time.

The Boltzmann integral, Eq. (1), may be expressed as

$$\sigma(t) = \int_{o}^{t} G(t-u) \frac{d\epsilon(u)}{du} du \tag{41}$$

by making a change of variables and noting in Eq. (40) that $dG(t)/dt = \Omega(t)$. When the ramp excitation,

$$\epsilon(t) = \dot{\epsilon}_o th(t) - \dot{\epsilon}_o (t - t_1) h(t - t_1) \tag{42}$$

is substituted into Eq. (41) we obtain

$$G_M(t) = \sigma(t)/\epsilon_o = \frac{1}{t_1} \int_{t-t_1}^{t} G(u)\, du \tag{43}$$

where G(t) is the actual shear relaxation modulus, and $G_M(t)$ is the measured shear modulus. A fairly representative analytical expression for G(t) is the power law approximation (3)

$$G(t) = G_e + \frac{G_g - G_e}{(1 + t/t_o)^n} \tag{44}$$

where G_e is the equilibrium modulus, G_g is the glassy modulus, t_o is a characteristic time constant, and n is a characteristic exponent. This expression is plotted in Fig. 7b logarithmically as a function of t/t_o using the typical values of G_g = 10,000 bars, G_e = 10 bars,

and n = 2/3. Substituting Eq. (44) into Eq. (43) and integrating yields

$$G_M(t) = G_e + \frac{G_g - G_e}{(1 - n)} \frac{t_o}{t_1} \left[\left(1 + \frac{t}{t_o}\right)^{1-n} - \left(1 + \frac{t - t_1}{t_o}\right)^{1-n} \right] \qquad (45)$$

The error resulting from using the ramp function, $(G_M - G)/G$, is plotted as a function of t/t_1, for various values of t_o/t_1 in Fig. 7a. It is seen that the largest error is around 1% for lag times of $25t_1$ for t_o/t_1 ratios between 0.001 and 10. For shorter lag times the error rises steeply, the closer the rise time t_1 is to the characteristic relaxation time t_o. Experimentally, this was evident by the lack of superposition of the initial portions of the curves in the middle of the transition region. Consequently, these portions of the curves were discarded (cf. Figs. 8, 9, 12, 13 and 18). Calculations were also performed for n = 1/2 and n = 3/5. The results were not significantly different and are not reported.

3.2 Temperature and Pressure Dependence of the Time-dependent Young's Modulus, E(t)

For isothermal-isobaric segments of E(t) to superpose by horizontal shifts along the logarithmic time axis it is necessary that changes in temperature and pressure affect all relaxation times in the same manner. This is a necessary, but not a sufficient condition. In addition, the effect of temperature and pressure on the modulus at any fixed time must be known to allow correction of the

isothermal-isobaric segments before shifting.

It is shown in elasticity theory that the elastic Young's modulus, E, is given in terms of the elastic shear and bulk modului, G and K, by

$$E = \frac{9KG}{3K + G} \tag{46}$$

Since the Young's modulus is thus a combination of the two fundamental moduli, G and K, which refer to changes in shape and size, respectively, we must examine the temperature and pressure dependence of these moduli to understand that of the Young's modulus, E.

The temperature and pressure dependence of the bulk modulus is found to be described by

$$K(T, P) = K^*(T) + kP$$

$$K^*(T) = K^*_o \exp\left[-m\alpha^* (T - T_o)\right] \tag{47}$$

where $K^*(T)$ is the bulk modulus at zero pressure, α^* is the thermal expansivity at zero pressure, and k and m are material parameters. K^*, k, and α usually assume different values for the rubbery and glassy states, whereas m is found to be constant (37). Equation (47) can be integrated to give the temperature and pressure dependence of the volume, cf. Section 4.11.

The statistical theory of rubber elasticity predicts the

temperature and pressure dependence of the shear modulus to be

$$G(T,P) = G(T_o,P_o)\,\rho\,T/\rho_o T_o \tag{48}$$

where $G(T_o,P_o)$ is the modulus at temperature T_o and pressure P_o. Sharda (57) has recently shown ρ/ρ_o to over correct the effect of pressure on G; for natural rubber the effect of pressure on the shear modulus is correctly given by

$$G(P) = G(P_o)\,J^{-\gamma} \tag{49}$$

where $G(P_o)$ is the shear modulus at zero pressure, $J = V/V_o = \rho_o/\rho$ and γ is a material parameter whose value is 0.2 for natural rubber. Since the volume is also dependent on the temperature, this result may be extended to include the effect of temperature on the density, i.e. $J = J(T,P)$. The integrated form of Eq. (47) may be employed for this purpose, cf. Section 4.11. We therefore write

$$G(T,P) = G(T_o,P_o)\,J^{-\gamma}T/T_o \tag{50}$$

In practice this effect is found to be quite small.

In the transition and glassy regions the effects of temperature and pressure on the shear modulus are not known. In the rubbery region it is reasonable to assume that $G \ll K$ i.e. that the rubber is incompressible. In this case $E = 3G$ and any temperature and pressure dependence of E will be the same as that of G. This assumption can not be made in the transition and glassy regions.

Measurements of the time-dependent shear modulus, G(t), would have afforded an easier reduction of the data since the effect of pressure on the modulus at fixed time would not have to be taken into account, i.e. the effect predicted by Eq. (50) is almost negligible for the pressures less than 5 kbar. However, experimentally the determination of G(t) under hydrostatic pressure is more difficult than that of E(t). We thus examine the effect of K on E.

For a linear viscoelastic material the constants E, G, and K in Eq. (46) must be replaced by their Carson transforms (the s-multiplied Laplace transforms). We thus have

$$\bar{E}(s) = \frac{9\bar{K}(s)\,\bar{G}(s)}{3\bar{K}(s) + \bar{G}(s)} \tag{51}$$

Equation (51) may be simplified by noting that the time dependence of the bulk modulus K(t) is negligible compared to the time dependence of G(t) or E(t); time dependent measurements of the bulk modulus by McKinney and coworkers showed K(t) to increase only by approximately 50% from rubbery to glassy behavior (39), whereas the shear modulus increases by three orders of magnitude. Assuming the bulk modulus to be independent of time, we have $\bar{K}(s) = K/s$ and Eq. (51) may be rewritten as

$$\bar{E}(s) = \frac{\bar{G}(s)}{1 + s\bar{G}(s)/3K} \tag{52}$$

where K is independent of time but dependent on temperature and

pressure. We now compare $\overline{E}_o(s)$, the Young's modulus at zero pressure, to $\overline{E}_p(s)$, the Young's modulus at pressure P, and assume $\overline{G}_o(s) = \overline{G}_p(s)$ based on the results of Eq. (50). Equation (52) becomes

$$\overline{E}_o(s) = \overline{E}_p(s) + \frac{1}{9}\left(\frac{1}{K_p} - \frac{1}{K^*}\right) s\overline{E}_o(s)\,\overline{E}_p(s) \tag{53}$$

Inverting Eq. (53) yields

$$E_o(t) = E_p(t) + \frac{1}{9}\left(\frac{1}{K_p} - \frac{1}{K^*}\right) E_g E_p(t) + \int_o^t E_p(t-u)\, dE_o(u) \tag{54}$$

where K_p is the pressure dependent bulk modulus given by Eq. (47). The Stieljes convolution integral in Eq. (54) can be evaluated numerically if $E_p(t)$ and $E_o(t)$ are known for all times. However, we do not know this information until we have applied time-pressure superposition to the data. We therefore examine the possibility of converting E(t) into G(t) at each pressure, and then utilizing Eq. (50) for reducing the shear modulus at elevated pressures to atmospheric pressure.

Equation (52) may be written in terms of the shear modulus

$$\overline{G}(s) = \frac{\overline{E}(s)}{3\left[1 - s\overline{E}(s)/9K\right]} \tag{55}$$

where K is given by Eq. (47). We first examine the limits of Eq. (55) by writing Eq. (2) in terms of Young's modulus, and taking the Laplace transform,

$$\bar{E}(s) = E_e/s + \sum_p \frac{E_p \tau_p}{1 + \tau_p s} \tag{56}$$

where E_e is the equilibrium Young's modulus. We see that for long times, i.e. for $s \longrightarrow 0$, $s\bar{E}(s)/9K$ reduces to $E_e/9K$ which is of the order of 10^{-4}. Hence, in the rubbery region

$$\bar{G}(s) = \bar{E}(s)/3 \qquad (s \longrightarrow 0) \tag{57a}$$

or

$$G(t) = E(t)/3 \qquad (t \longrightarrow \infty) \tag{57b}$$

At short times, i.e. for $s \longrightarrow \infty$

$$s\bar{E}(s) = E_e + \sum_p E_p = E_g \tag{58}$$

where E_g is the glassy Young's modulus. Hence, $sE(s)/9K$ reduces to $E_g/9K$ which is of the order of 0.1 since $E_g \approx K$. Therefore

$$\bar{G}(s) \approx \bar{E}(s)/2.7 \qquad (s \longrightarrow \infty) \tag{59a}$$

or

$$G(t) \approx E(t)/2.7 \qquad (t \longrightarrow 0) \tag{59b}$$

It is erroneous, however, to infer that for $0 < t < \infty$, the proportionality constant between E(t) and G(t) must lie between 2.7 and 3.0. We proceed to demonstrate this.

Unfortunately, Eq. (55) can not be inverted. A reasonable

approximation may be obtained by expanding the denominator and neglecting higher order terms. This yields

$$\overline{G}(s) = \overline{E}(s) \quad [1 + s\overline{E}(s)/9K] \, /3 \tag{60}$$

which may be inverted to give

$$G(t) = \frac{E(t)}{3} \, (1 + E_g/9K) + \frac{1}{27K} \int_o^t E(t - u) \, dE(u) \tag{61}$$

Again, as in Eq. (54), the Stieljes convolution integral can be evaluated numerically once E(t) is known for all times. However, we do not have this information until the data have been reduced, and time-temperature or time-pressure superposition applied to them. We therefore seek an alternate method. Furthermore, we chose to reduce the data in terms of the time-dependent shear modulus, G(t).

Noting that $s\overline{E}(s)/9K$ varies approximately between 10^{-4} and 10^{-1}, we seek a useable approximation by writing

$$G(t) = \frac{E(t)}{3[1 - E(t)/9K]} \tag{62}$$

To check the validity of this assumption, and to gain intuition for the relative error which may result, we apply the simple 3-parameter Maxwell model

$$\overline{E}(s) = E_e/3 + \frac{(E_g - E_e) \, \tau}{1 + \tau s} \tag{63}$$

which is simply Eq. (56) for a single relaxation time, and $E = E_g - E_e$. Substituting Eq. (63) into Eq. (55) and inverting yields the exact conversion

$$G_{55}(t) = E_e/3 + \frac{1}{3}\left[\frac{E_g}{1 - x} - E_e\right] \exp\left(\frac{-t/\tau}{1 - x}\right) \qquad (64)$$

where $x = E_g/9K$ and the subscript on G(t) denotes the corresponding equation from which the shear relaxation modulus was obtained. Equation (64) may be compared with the approximate conversion

$$G_{60}(t) = E_e/3 + \frac{\left(E_g - E_e\right)}{3}\left[1 + x(1 - t/\tau)\right] \exp\left(-t/\tau\right) \qquad (65)$$

obtained by substituting Eq. (63) into Eq. (60) and inverting. In addition we have $G_{57}(t)$ obtained from Eq. (57), and finally the new proposed approximation $G_{62}(t)$. Table I shows values of the various shear relaxation moduli obtained in the indicated way for $x = 0.1$ and $x = 0.05$, with the typical parameters $E_e = 10$ bar, and $E_g = 10,000$ bar.

The ratio $\log G_{62}/G_{55}$, representing the deviation of the approximation from the exact conversion, has a maximum around $t/\tau = 6$ for the simple model and the parameters chosen. We conclude that G_{62} is a reasonable approximation to G(t) but we may expect that vertical shifts will be necessary in the transition region when applying time-temperature, or time-pressure, superposition to the data. These shifts result from the error in calculating G(t).

TABLE I

Values of Shear Modulus, G(t), Calculated from Equations Noted

$X = 0.1$

t/τ	0.01	0.10	0.5	0.8	1.0	2.0	4.0	6.0	8.0	12.0
$G_{55}(t)$	3659	3315	2126	1525	1221	404	46.8	8.04	3.84	3.34
$G_{60}(t)$	3627	3288	2124	1530	1228	409	46.0	7.46	3.67	3.33
$G_{62}(t)$	3662	3316	2155	1568	1275	460	64.4	11.59	4.45	3.35
$G_{57}(t)$	3300	3016	2023	1500	1228	454	64.3	11.59	4.45	3.35
$\log\frac{G_{62}}{G_{55}}$	.0004	.001	.006	.012	.019	.056	.139	.159	.064	.002

$X = 0.05$

t/τ	0.01	0.10	0.5	0.8	1.0	2.0	4.0	6.0	8.0	12.0
$G_{55}(t)$	3469	3155	2072	1512	1226	430	55.3	9.66	4.10	3.35
$G_{60}(t)$	3463	3152	2074	1515	1228	431	55.1	9.52	4.06	3.34
$G_{62}(t)$	3472	3159	2086	1534	1251	457	64.4	11.59	4.45	3.35
$G_{57}(t)$	3300	3016	2023	1500	1228	454	64.3	11.59	4.45	3.35
$\log\frac{G_{62}}{G_{55}}$	.0004	.0006	.003	.006	.008	.026	.066	.079	.035	.001

We assume that the effect of this error on the shapes of the curves is negligible. This assumption was partially checked out by comparing the shapes of $G_{57}(t)$ and $G_{62}(t)$; no difference was detected. Once the master curve is obtained, we may obtain $G_{60}(t)$. However, since we have fixed the asymptotic behavior of G(t), we have, essentially, empirically incorporated Eq. (55) into our data reduction scheme by allowing the additional vertical shifts in the transition region. Therefore, nothing would be gained by calculating $G_{60}(t)$

The most significant result of the above analysis is that it shows that the short time behavior has a profound influence on the conversion from E(t) to G(t). It is generally assumed that the time-dependent shear modulus is simply 1/3 the time-dependent Young's modulus for the region where $E(t) << 9K$. We have shown this to be a poor assumption, except in the limit as time approaches infinity, i.e. the rubbery region, which is the region of equilibrium, or purely elastic response. Thus, the time-dependent shear and Young's moduli are not simply related.

The simple model represented by Eq. (63) is a special case. However, all of the short time response in the conversion to G(t) may be seen by noting that we may replace $s\bar{E}(s)$ in Eq. (55) by $E_g + \bar{\dot{E}}(s)$ to give

$$\bar{G}(s) = \frac{\bar{E}(s)}{3\left[1 - \frac{E_g + \bar{\dot{E}}(s)}{9K}\right]} \tag{66}$$

where, from Eq. (56), we have

$$\bar{\dot{E}}(s) = -\sum_p \frac{E_p}{1 + \tau_p s} \tag{67}$$

Thus, $\bar{\dot{E}}(s)$ is negative and is always smaller than E_g. Hence, no matter what the functional form of $\bar{E}(s)$, $\bar{G}(s)$ will depend on the magnitude of E_g.

A more sophisticated model than that represented by Eq. (63) might show larger or smaller errors in the conversion from E(t) to G(t) by the use of the approximation given by Eq. (62).

3.3 Experimental Results

The experimentally measured quantities are the strain, $(L - L_o)/L_o$, and the time dependent force, f(t). The stress is determined by dividing the force by the cross-sectional area of the specimen. The thermal expansivity and the isothermal compressibility are used to correct the initial cross-sectional area of the specimen to the area existing at the experimental temperature and pressure. The time-dependent Young's modulus,

$$E(t) = \sigma(t)/\varepsilon_o \tag{68}$$

is then calculated and substituted, together with the bulk modulus, Eq. (47), into Eq. (62) to yield the time-dependent shear modulus, G(t), at the temperature and pressure of the experiment.

Equation (32) is found to describe the temperature and pressure dependence of the bulk modulus remarkable well. It is discussed more thoroughly in Chapter 4. As the values of K* and k were not known for Hypalon and Viton, they were assumed to be identical with those for Neoprene which were obtained from the data of Weir (55). The compressibility data (the bulk modulus is the inverse of the compressibility) of Weir for four different elastomers were quite similar in both shape and magnitude. This lends support to the assumption. The values used for the various parameters are given in Table II of Chapter 4.

To apply time-temperature-pressure superposition to G(t), we must, before applying the shifting procedure, remove the effects of temperature and pressure on the modulus at fixed time. In Section 1.3 it was noted that the elastic response of the rubber is dominated by the configurational entropy of the system. The configuration entropy is directly affected by the temperature, and indirectly by the effect of temperature and pressure on the density of the material as shown by Eq. (50). We further noted that the internal energy becomes the controlling mechanism in the glassy state. It follows that some combination of the two mechanisms will influence the transition region. Finally, current theory (see Chapter 1) describes behavior only in the rubbery region and at most the initial portion of the transition region. We therefore expect that vertical shifts of the isothermal-isobaric segments of G(t) will be

necessary in the transition and glassy regions to allow for a shift from entropy controlled to internal energy controlled behavior as one approaches the glassy state. It is important to realize that these shifts are independent of the vertical shifts resulting from the error in the conversion to the shear modulus discussed in Section 3.2.

This expectation was born out experimentally. To empirically shift the segments along the logarithmic time axis, all measured shear moduli, G(t), were adjusted using Eq. (50). This scheme worked well in the rubbery and initial transition regions. However, as the glassy response was approached, superposition was unsatisfactory unless additional vertical shifts were allowed. Since no theory exists for this region and since we anticipate error in the magnitude of G(t), vertical shifts were admitted in the transition and glassy regions; the criterion being best superposition of the segments. This is consistent with the primary assumption that all relaxation times are affected similarly by a change in temperature or pressure, and that the error in G(t) does not affect the shapes of the segments. The resulting shear modulus becomes

$$G_r(t) = (T_o J^{\gamma} G(t)/T) \Delta G_{cor} \qquad (69)$$

where $G_r(t)$ is the reduced shear modulus and ΔG_{cor} is the empirical vertical shift. These shifts are plotted in Figs. 16 and 17 for Hypalon-40 and Viton-B, and are further discussed in Section 3.33. No empirical vertical shifts were needed on Neoprene and

EPDM data (Appendix B).

It should be noted that the empirical vertical shifts are not arbitrary. Since the isothermal-isobaric segments of G(t) are smooth, there exists only one point in the log modulus-log time plane that gives a good superposition of the segments. Furthermore, since two mastercurves are constructed, one from time-temperature superpositioning and a second from time-pressure superpositioning, the shifting procedure must be consistent; otherwise the two master curves will be different. The empirical vertical shifts are thus regarded to reflect real material behavior (except for any portion of the shift which arises from the conversion technique). Direct measurements of G(t) as a function of both temperature and pressure could therefore yield background data for the development of a theory accounting for changes resulting from shifting from entropy to internal energy controlled behavior.

3.31 Hypalon-40

The reduced isothermal-isobaric segments, $G_r(t)$, are plotted in Figs. 8 and 9 for Hypalon-40. Figure 8a shows data obtained at 25°C as a function of pressure. Figures 8b, 9a and 9b show data obtained at 1, 1,000, and 2,000 bar, respectively, as functions of temperature. The plus sign (+) indicates the first segment for which an additional shift, $\log \Delta G_{cor}$, was made. The arrow indicates the first segment which deviates from the prediction

based on the free volume approach discussed in Chapter 4; it may be thought of as representing the onset of glassy behavior. Figure 10 shows two master curves obtained by empirical vertical and horizontal shifting.

The empirical horizontal shifts are recorded as $\log a_{25.0,P}$ and are plotted in Fig. 10b. Master curve B is obtained from Fig. 8b. The empirical horizontal shifts are recorded as $\log a_{T,1.0}$ and are plotted in Fig. 11b. Thus, the reduced modulus, $G_R(t)$ in Fig. 10a, is related to $G_r(t)$ by

$$G_R(t) = G_r(t/a_{T,P}) \tag{70}$$

Both curves contain the same information, i.e. the time dependence of the shear relaxation modulus over 12 decades of time at $T = 25.0^{\circ}C$ and $P = 1.0$ bar. There coincidence in the rubbery and in most of the transition region indicates the material to be piezo-and thermo-rheologically simple. The slight difference in the glassy region is not suprising. Glasses formed by the application of pressure are generally found to be denser that those formed by lowering the temperature (34, 38, 53, 54). We would expect the denser glass to display the greater shear modulus. The empirical vertical shifts are plotted in Fig. 16.

Figure 11a shows the three master curves obtained by shifting the segments of Figs. 8b, 9a, and 9b, respectively. All three curves are reduced to the reference temperature of $25.0^{\circ}C$, but left at the

respective experimental pressures. The three master curves may easily be brought into superposition by applying the shift factors of Fig. 10b. Again the glasses formed at the elevated pressures are found to display higher moduli, respectively.

3.32 Viton-B

The measurements on Viton-B are presented in the same manner as are those on Hypalon-40. It is interesting that the materials share almost identical behavior with respect to a change in temperature as may be seen by comparing Figs. 8b and 12b. However, the effect of a change in pressure on Viton is twice the effect on Hypalon. Referring to Figs. 16 and 17, we also see that the empirical vertical shifts applied to the two materials are quite different. This difference will be discussed in the next section.

3.33 Empirical Vertical Shifting Behavior

The empirical vertical shifts, ΔG_{cor}, applied to the Hypalon and Viton data are ploted in Figs. 16 and 17, respectively. The shifts for pressures less than 2 kbar in Hypalon, Fig. 16, are not plotted since they are all zero. The arrows indicate the pressure or temperature at which the shift factors, $\log a_{T,P}$, deviate from the smooth curves in Figs. 10b, 11b, 14b, and 15b. This point, although not the glass transition, T_g, as defined in the classical sense (i.e. by volumetric measurements), may be thought of as the

onset of glassy behavior, and will be referred to here as the inflection temperature, T_I. In fact, it is undoubtedly closely related to T_g. All plots in Figs 16 and 17 are seen to be relatively smooth, and display a maximum in the vicinity of T_I. This maximum corresponds to both the maximum in log $G_{62}(t)/G_{55}(t)$ in Table II, which resulted from the error encountered in correcting to G(t), and to the region in which we expect the internal energy and configurational entropy mechanisms to contribute about equally.

The empirical vertical shifts for Viton, Fig. 17, are particularly interesting; the shifts resulting from reducing the pressure data exhibit a maximum, whereas the shifts resulting from the temperature data exhibit a minimum except at the higher pressures. Furthermore, the time-temperature data at the elevated pressures exhibit hardly any shifts at all, indicating internal consistency. The maximum at about 25°C in Fig. 17d corresponds to the maximum at 2 kbar in Fig. 17a.

We might expect that the simple 3-parameter Maxwell model assumed in Section 3.2 would always over predict the true value of G(t); this would result in all empirical vertical shift curves having the form of Fig. 17b. However, there are several explanations for the observed behavior: (1) the model represents the behavior of elastomers only in a general way; the response of a real material is quite different; (2) it was necessary to assume values of K* and k for

the bulk modulus from data on Neoprene. Since the ratio $E_g/9K$ strongly influences the vertical shift factors, we could have easily over or under predicted G(t); (3) even had we measured G(t) directly, thereby eliminating the above source of error, we still anticipate empirical shifts in this region due to the shift from a configurational entropy controlled to an internal energy controlled mechanism. Since the main objective is the investigation of the applicability of time-temperature-pressure superposition, we focus our attention on the horizontal shift factors, $\log a_{T,P}$, and lump the various contributions to the vertical shifts. To unscramble these contributions, we would need additional information which is not available at present. We emphasize that we have not violated our major assumption, that all relaxational processes are affected similarly by a change in temperature or pressure; as pointed out earlier, the vertical shifts are not arbitrary and have merely corrected for errors in our inability to correctly characterize the effect of temperature and pressure on the moduli.

3.34 Neoprene

The results on Neoprene are somewhat of a special case due to the high percentage of carbon black and clay filler (100 and 25 weight percent respectively). Neoprene was included in this study to determine whether any significant differences would arise in the behavior of a highly filled material. The behavior of highly filled

elastomers typically deviates from that of the pure elastomer in two major ways: (1) the entire master curve is shifted to higher moduli and to somewhat longer times, and (2) nonlinear stress-strain behavior is observed at much lower strains. The increase in modulus can be observed in Figs. 18 and 19. Both the rubbery and glassy response are almost twice that observed for the Hypalon and Viton.

Compressibility measurements by Weir (55) when plotted in terms of the bulk modulus and measurements of Young's modulus by Patterson (42) both showed the glass transition in Neoprene to occur at approximately 3.6 kbar pressure at 25°C. The relaxation curves in Fig. 18 seem to indicate that 4.6 kbar pressure still has not induced glassy behavior. However, the initial portions of the curves at the highest pressure tend to bend over. Furthermore, in Fig. 19b, a break in the shift factors, $\log a_{T,P}$, can be detected at about 3.8 kbar; the points above 3.8 kbar tend to form a straight line of different slope, similar to the behavior observed with Hypalon and Viton, Figs. 10b and 14b.

No empirical vertical shifts were made to obtain the master-curve in Fig. 19a. The resulting mastercurve is quite smooth in the initial portion of the transition region. We see poor superposition in and near the glassy region. Actually, this portion of the master-curve can be superposed quite well, if vertical shifts much larger than required with Hypalon and Viton, of the order of 0.35 log units,

are allowed. Had this been done, the break in the shift factors of Fig. 19b would also have disappeared. These vertical shifts were disallowed because they would have been arbitrary in view of the lack of curvature in the isothermal-isobaric segments of Fig. 18. Measurements at higher pressures than can be applied in the apparatus in its current form would possibly permit a resolution of this problem.

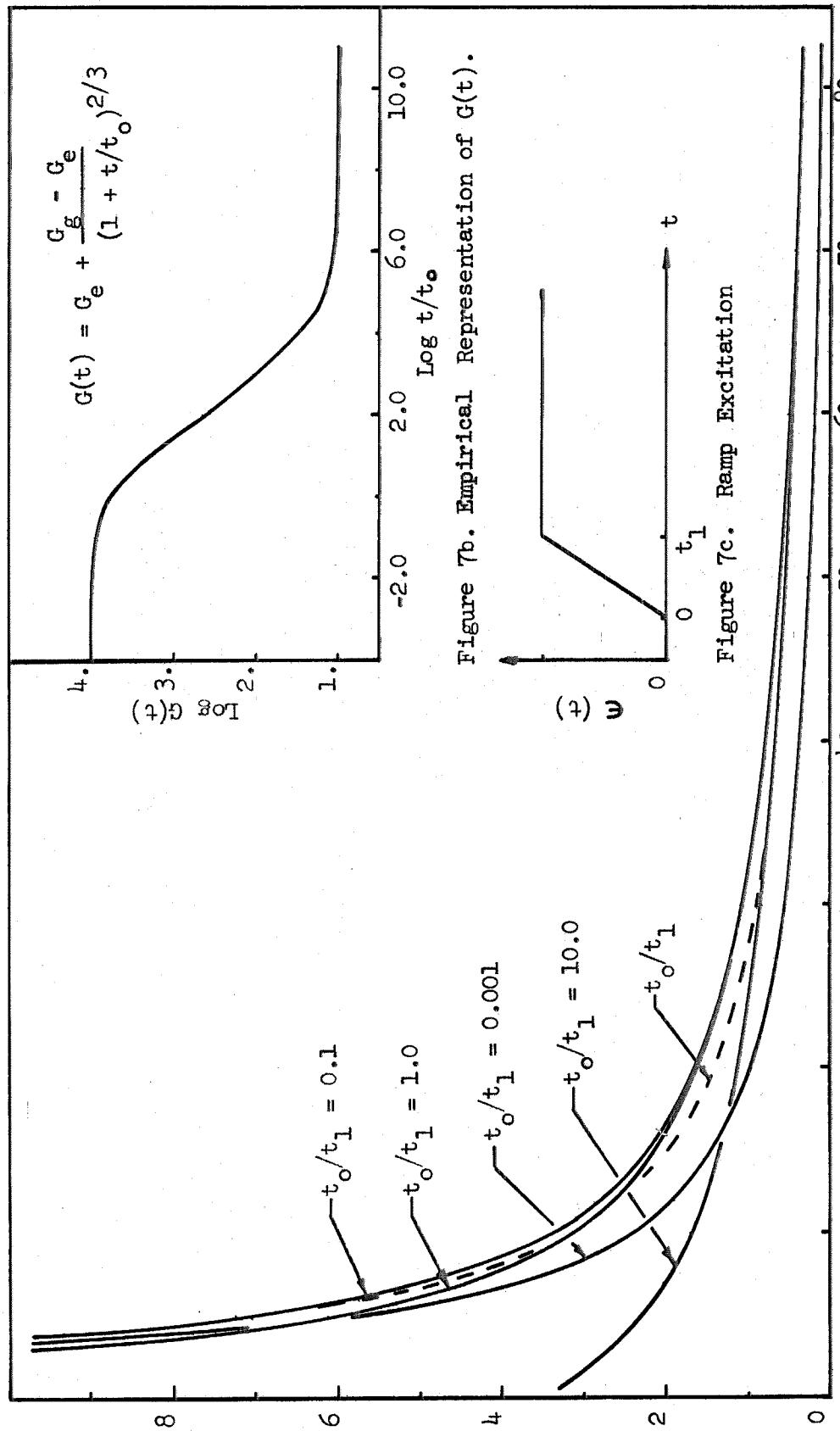

Figure 7b. Empirical Representation of G(t).

Figure 7c. Ramp Excitation

Figure 7a. Error Resulting from Approximating Step Function with Ramp Function, Fig. 7c, for Measuring Shear Modulus of Fig. 7b. Percent Error equals $(G_M - G)/G \times 100$.

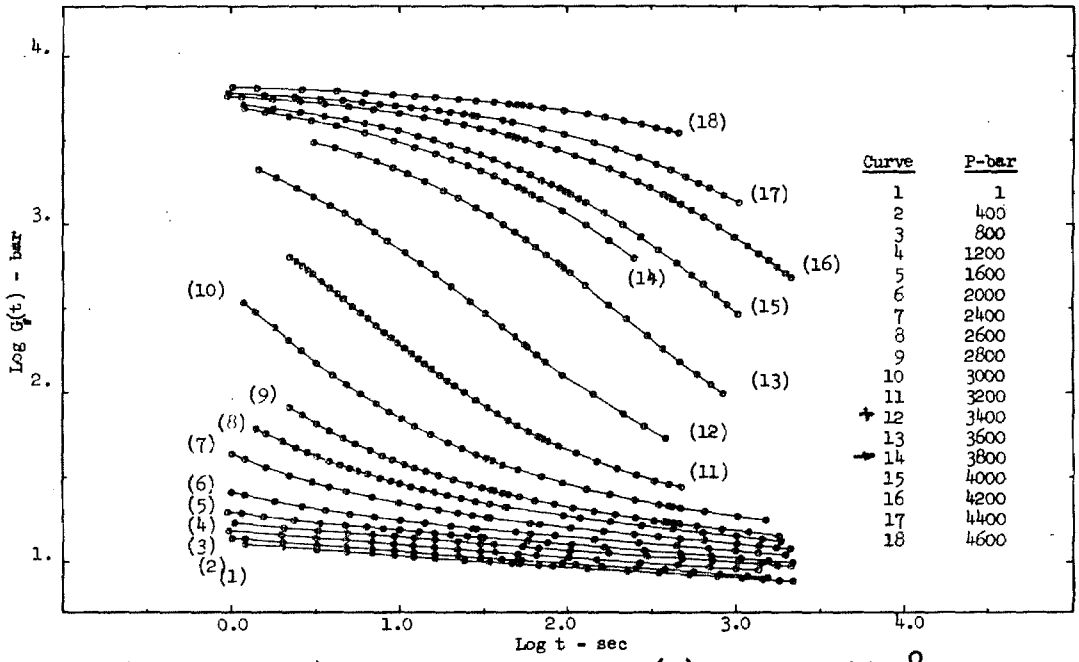

Figure 8a. Hypalon-40: Shear Modulus, $G_r(t)$, at T = 25.0°C and Pressures Indicated.

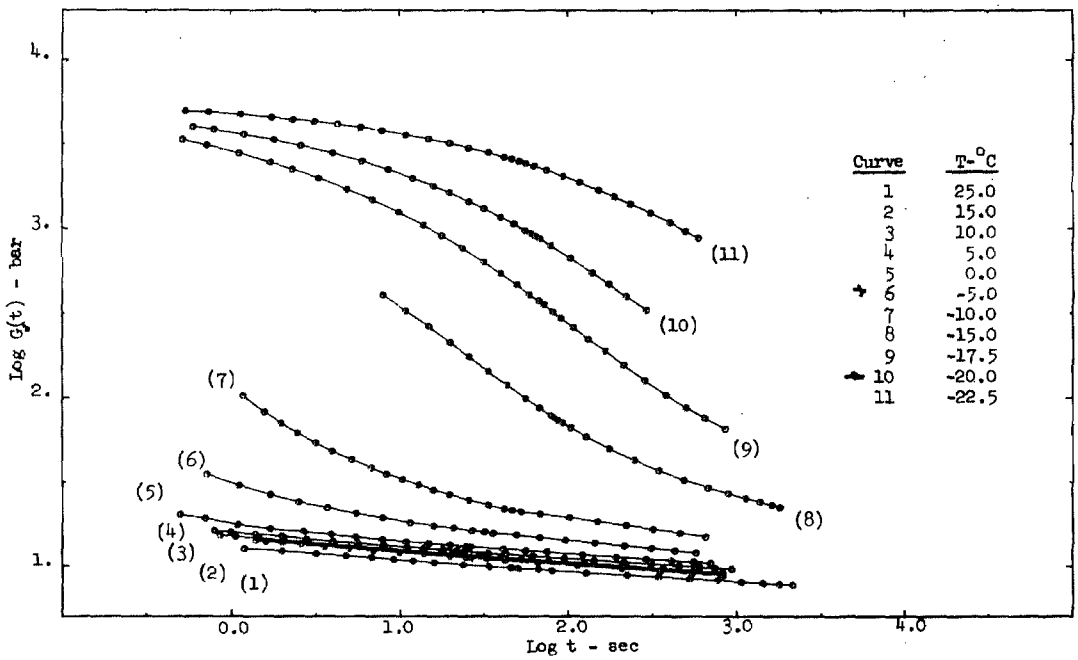

Figure 8b. Hypalon-40: Shear Modulus, $G_r(t)$, at P = 1.0 bar and Temperatures Indicated.

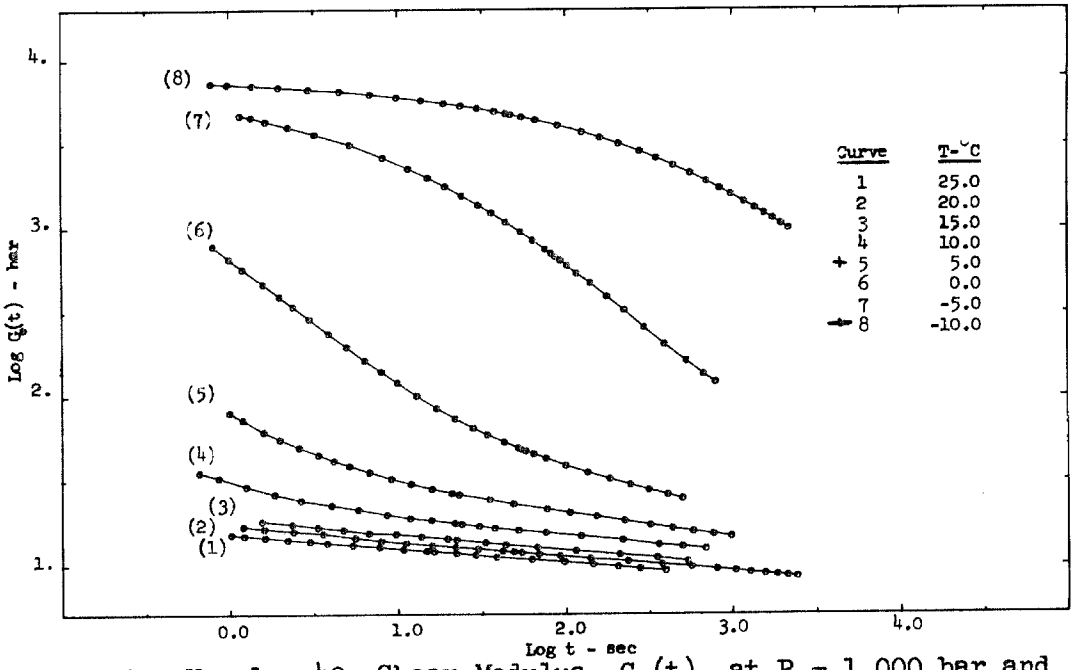

Figure 9a. Hypalon-40: Shear Modulus, $G_r(t)$, at P = 1,000 bar and Temperatures Indicated.

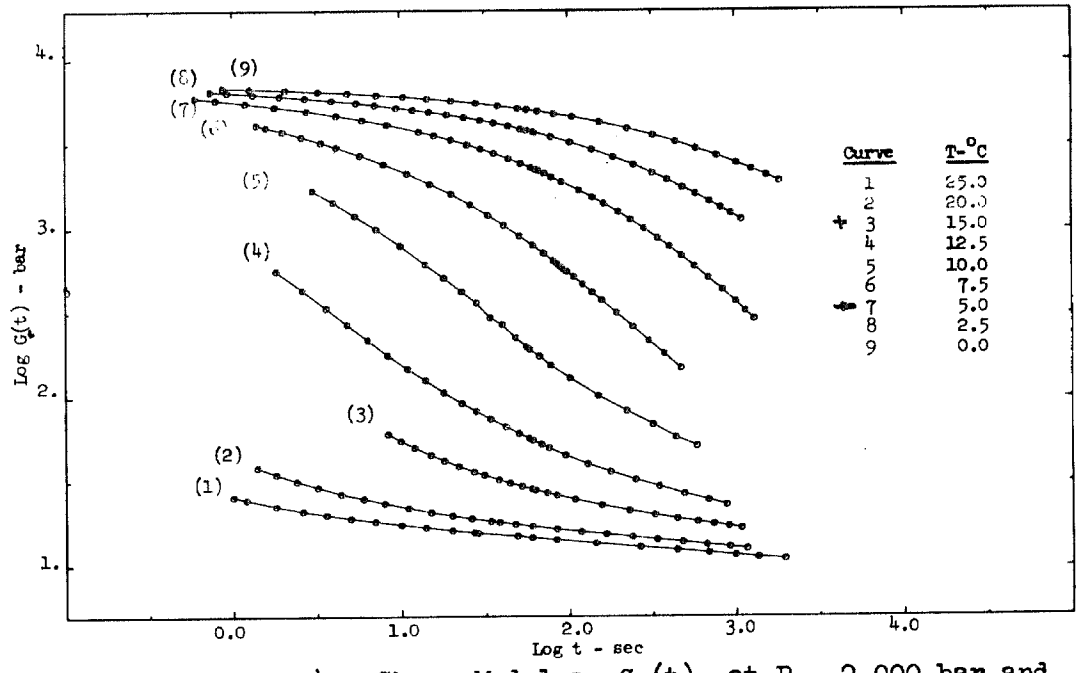

Figure 9b. Hypalon-40: Shear Modulus, $G_r(t)$, at P = 2,000 bar and Temperatures Indicated.

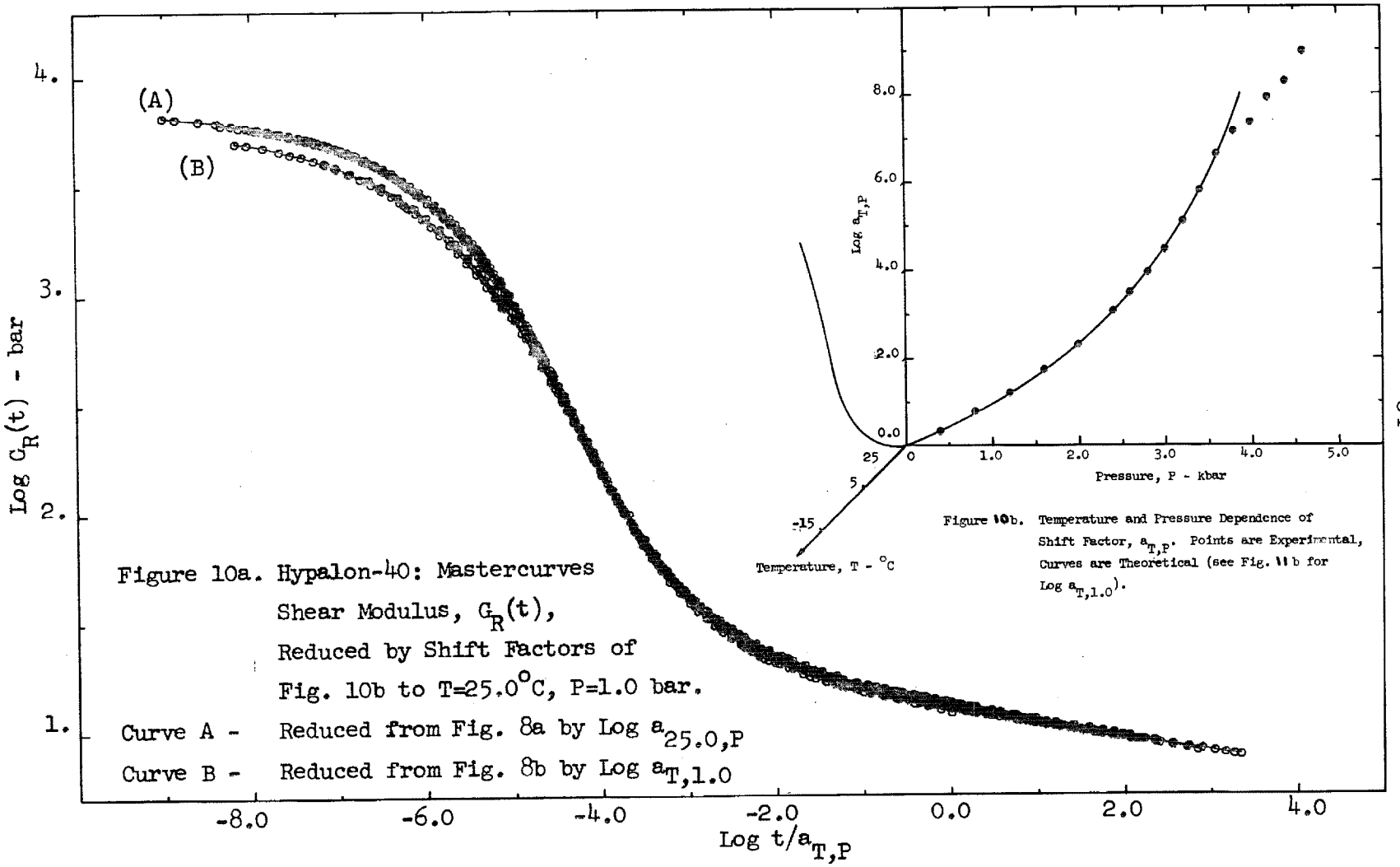

Figure 10a. Hypalon-40: Mastercurves Shear Modulus, $G_R(t)$, Reduced by Shift Factors of Fig. 10b to T=25.0°C, P=1.0 bar.

Curve A - Reduced from Fig. 8a by Log $a_{25.0,P}$

Curve B - Reduced from Fig. 8b by Log $a_{T,1.0}$

Figure 10b. Temperature and Pressure Dependence of Shift Factor, $a_{T,P}$. Points are Experimental, Curves are Theoretical (see Fig. 11b for Log $a_{T,1.0}$).

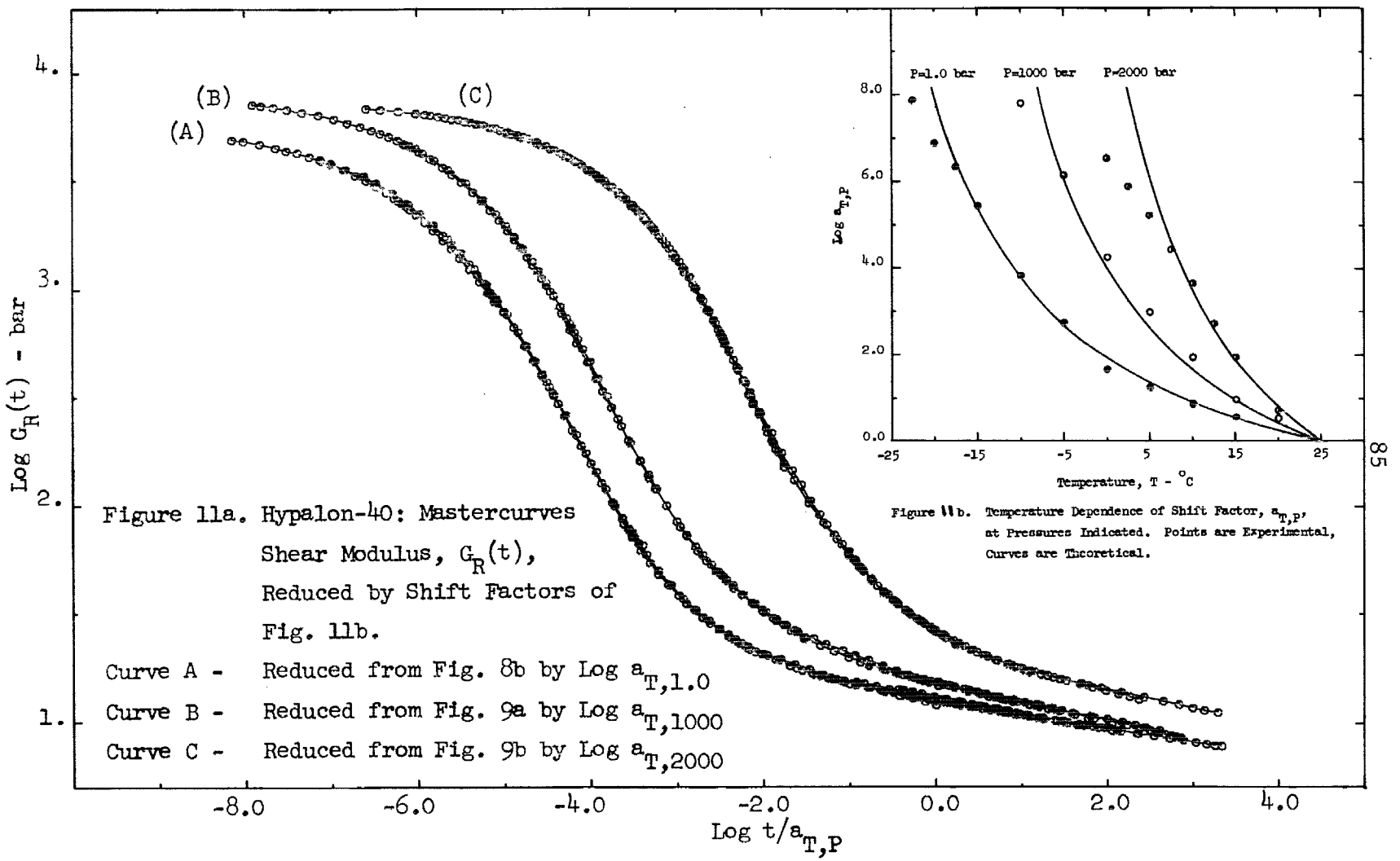

Figure 11a. Hypalon-40: Mastercurves Shear Modulus, $G_R(t)$, Reduced by Shift Factors of Fig. 11b.

Curve A - Reduced from Fig. 8b by Log $a_{T,1.0}$

Curve B - Reduced from Fig. 9a by Log $a_{T,1000}$

Curve C - Reduced from Fig. 9b by Log $a_{T,2000}$

Figure 11b. Temperature Dependence of Shift Factor, $a_{T,P}$, at Pressures Indicated. Points are Experimental, Curves are Theoretical.

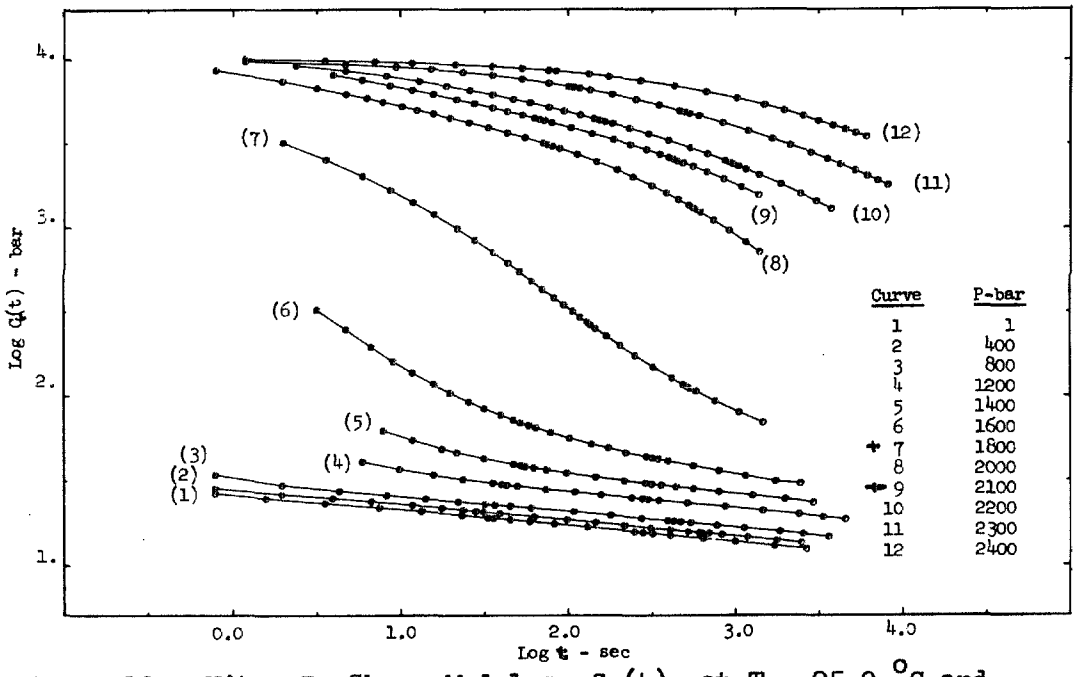

Figure 12a. Viton-B: Shear Modulus, $G_r(t)$, at T = 25.0 °C and Pressures Indicated.

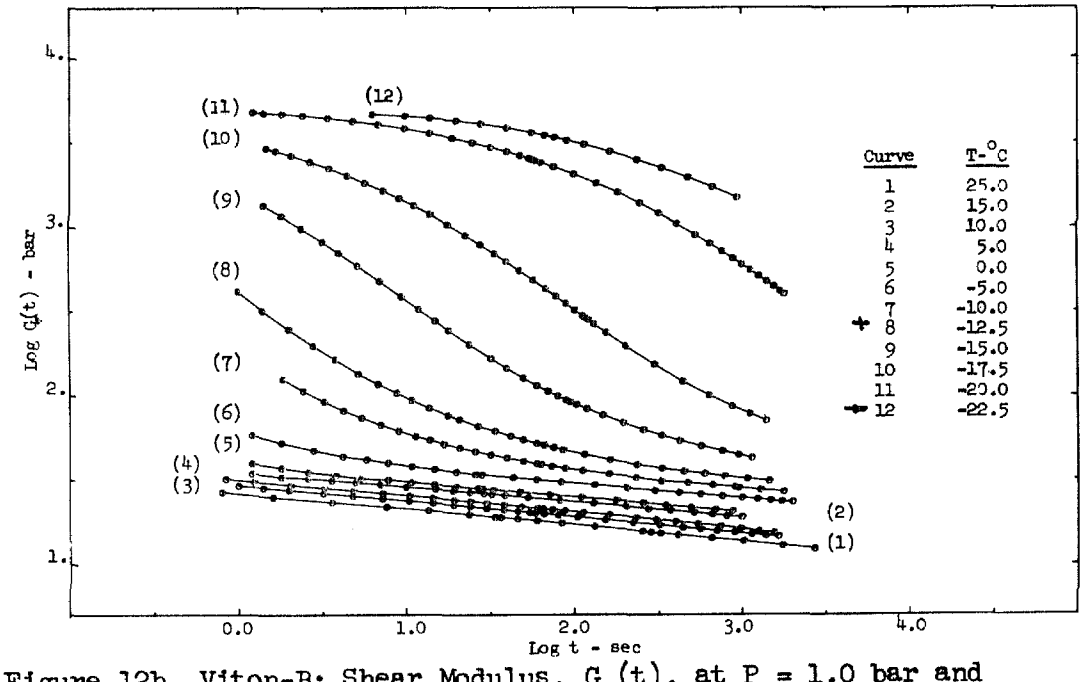

Figure 12b. Viton-B: Shear Modulus, $G_r(t)$, at P = 1.0 bar and Temperatures Indicated.

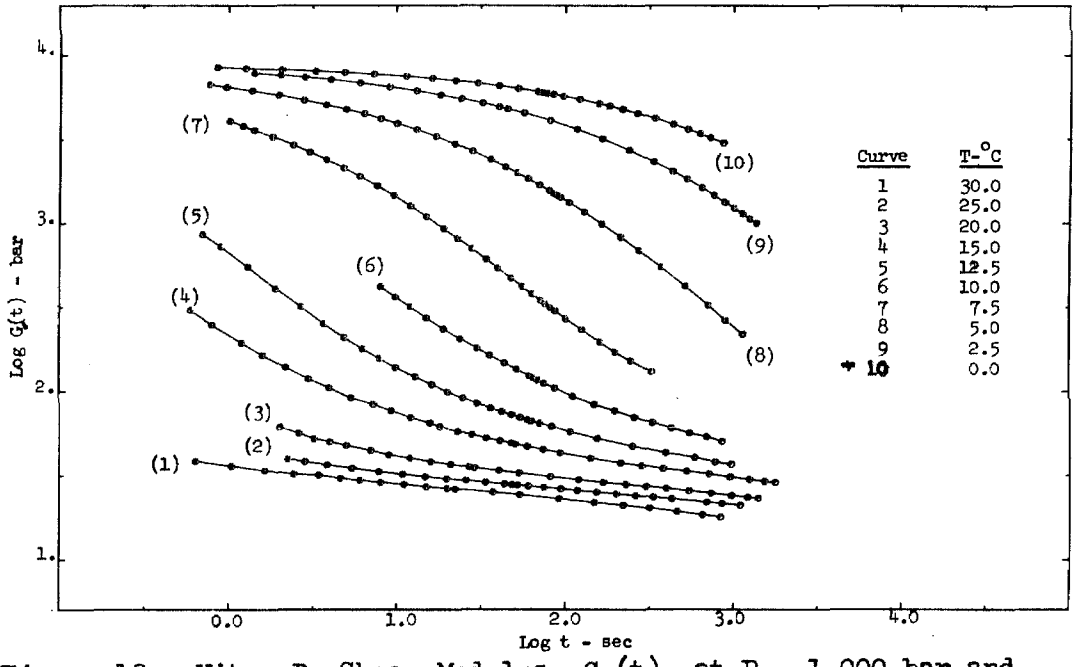

Figure 13a. Viton-B: Shear Modulus, $G_r(t)$, at P = 1,000 bar and Temperatures Indicated.

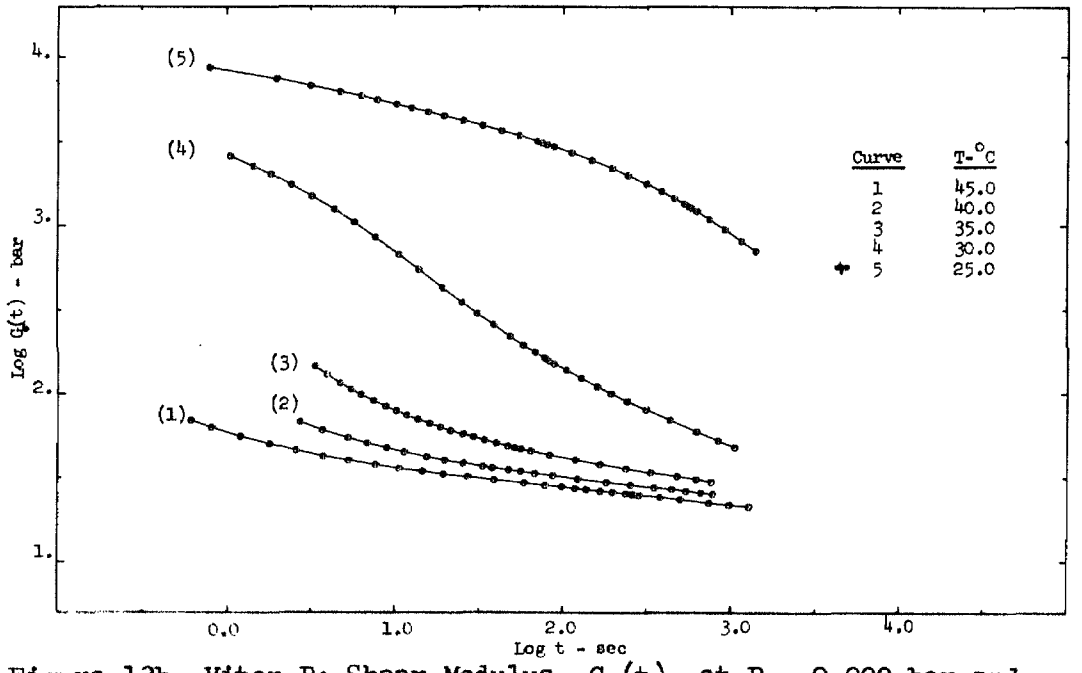

Figure 13b. Viton-B: Shear Modulus, $G_r(t)$, at P = 2,000 bar and Temperatures Indicated.

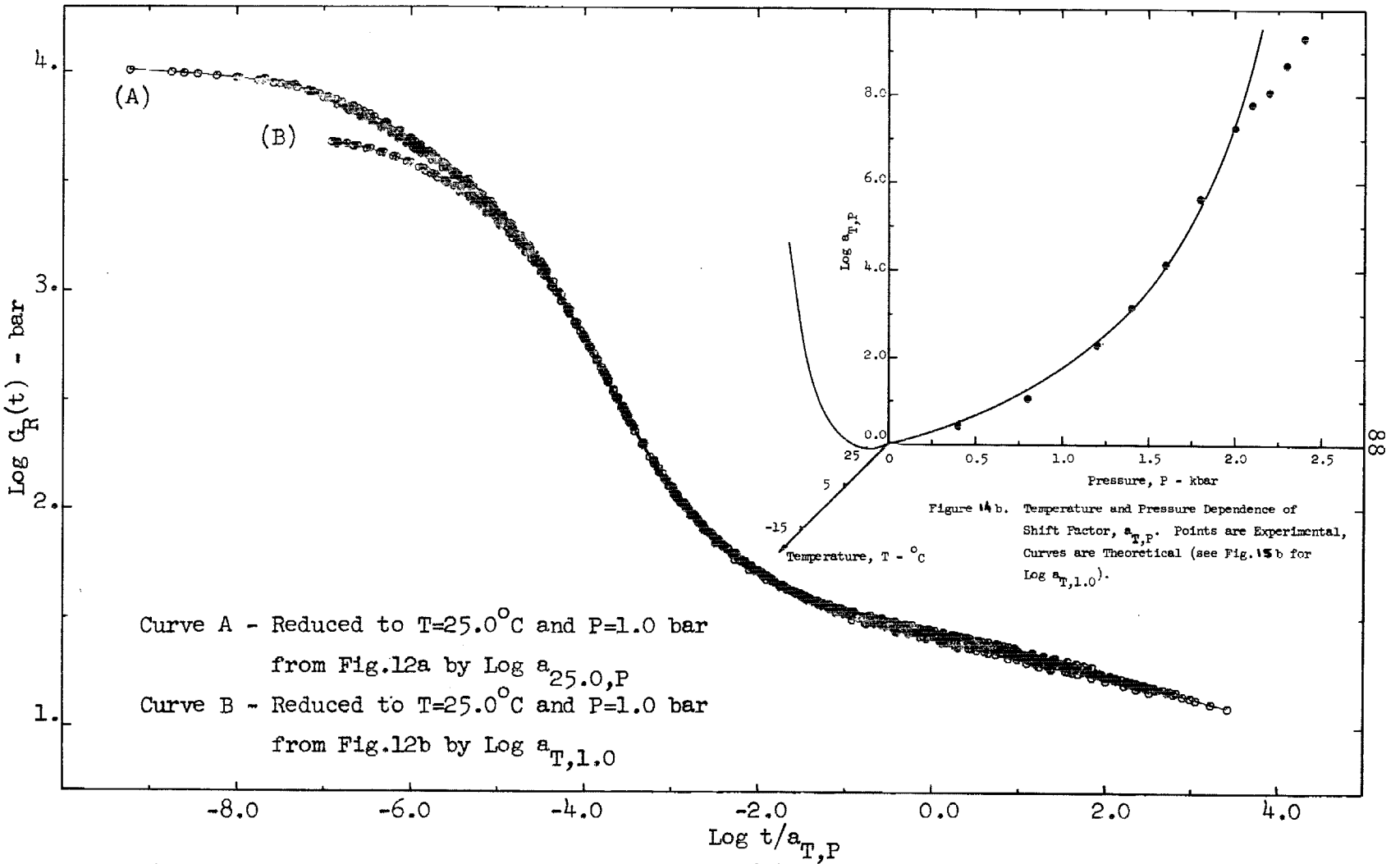

Figure 14b. Temperature and Pressure Dependence of Shift Factor, $a_{T,P}$. Points are Experimental, Curves are Theoretical (see Fig. 15b for Log $a_{T,1.0}$).

Figure 14a. Viton-B: Mastercurves. Shear Modulus, $G_R(t)$, Reduced by Shift Factors of Fig. 14b.

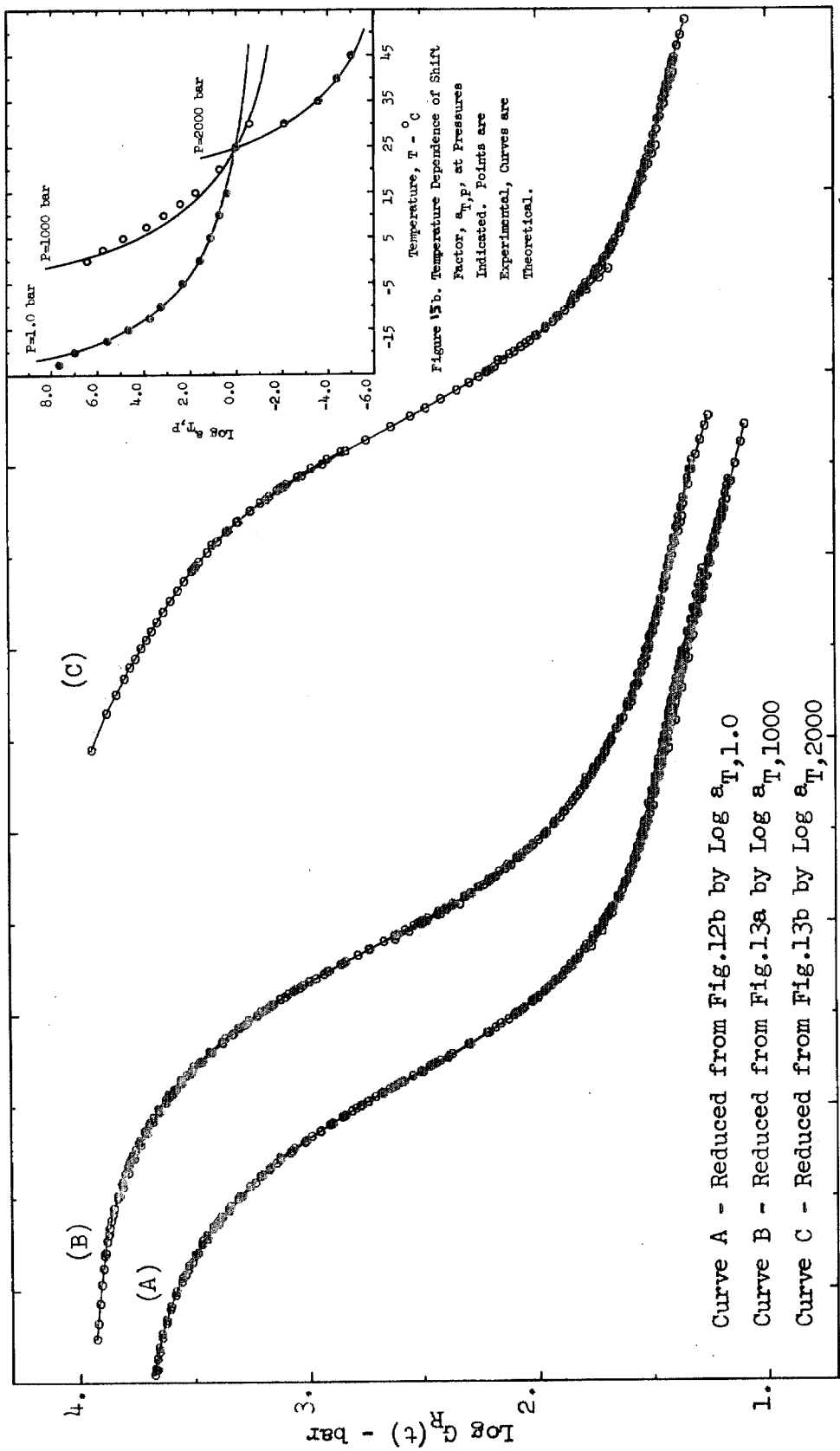

Figure 15a. Viton-B: Mastercurves. Shear Modulus, $G_R(t)$, Reduced by Shift Factors of Fig.15b.

Figure 15b. Temperature Dependence of Shift Factor, $a_{T,P}$, at Pressures Indicated. Points are Experimental, Curves are Theoretical.

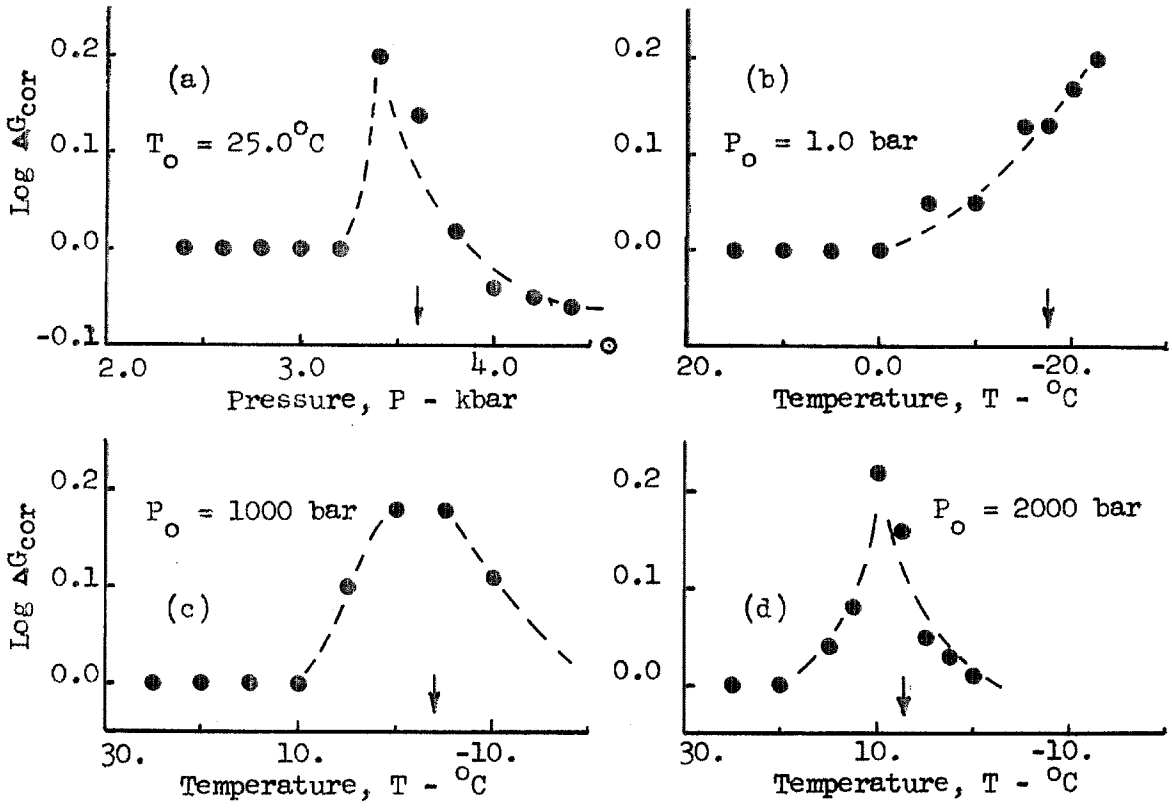

Figure 16. Hypalon-40: Vertical Shifts, Log ΔG_{cor}, Incorporated in Data Reduction. Arrows Indicate Onset of Glassy Behavior.

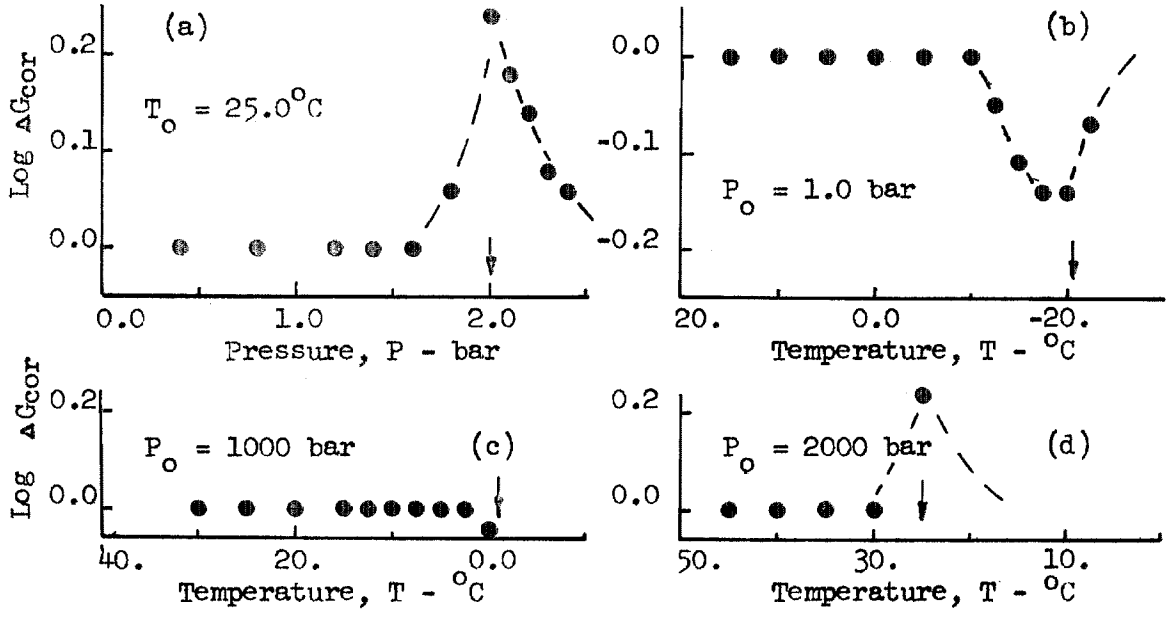

Figure 17. Viton-B: Vertical Shifts, Log ΔG_{cor}, Incorporated in Data Reduction. Arrows Indicate Onset of Glassy Behavior.

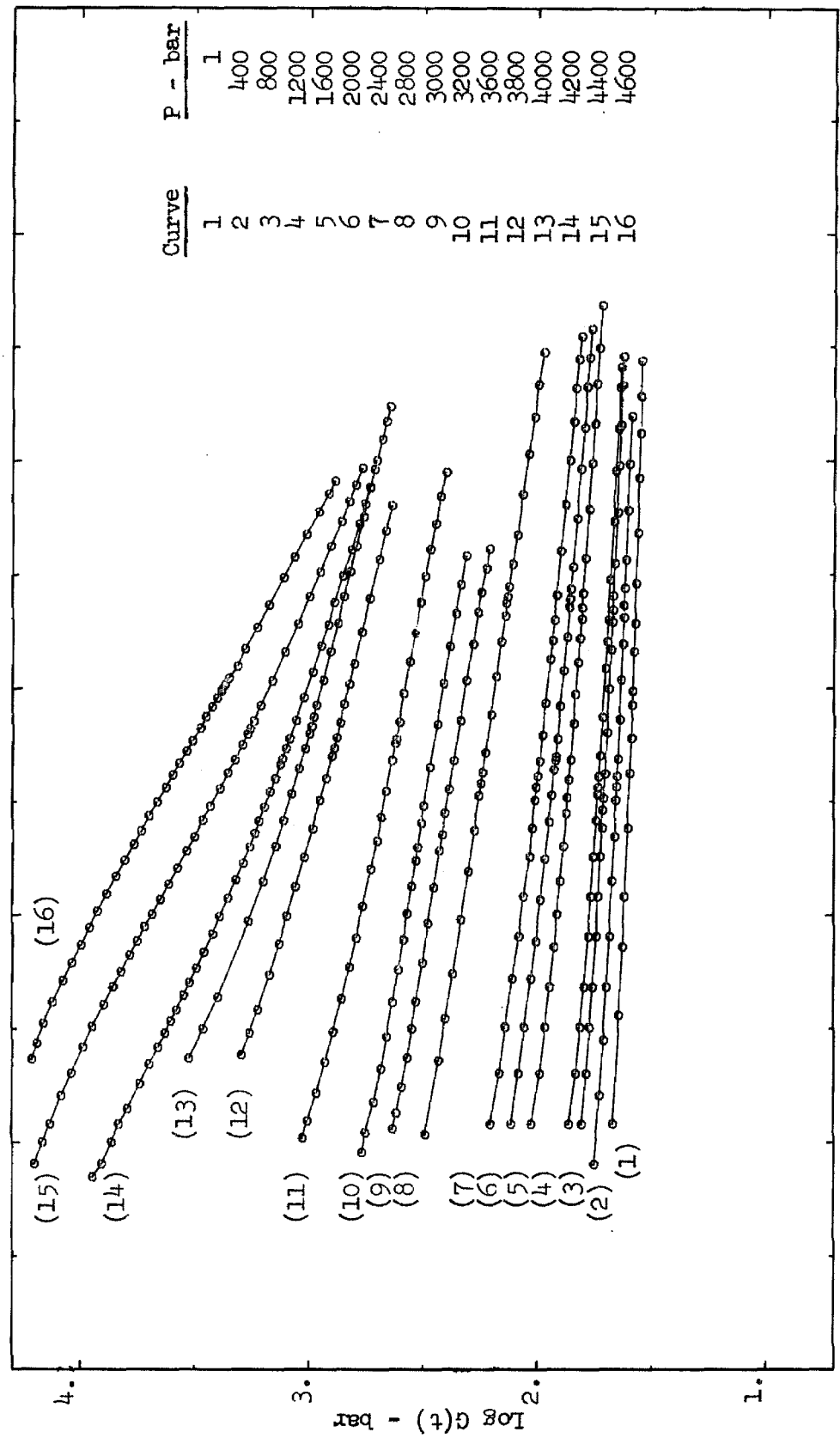

Figure 18. Neoprene: Shear Modulus, G(t), at T = 25.0°C and Pressures Indicated.

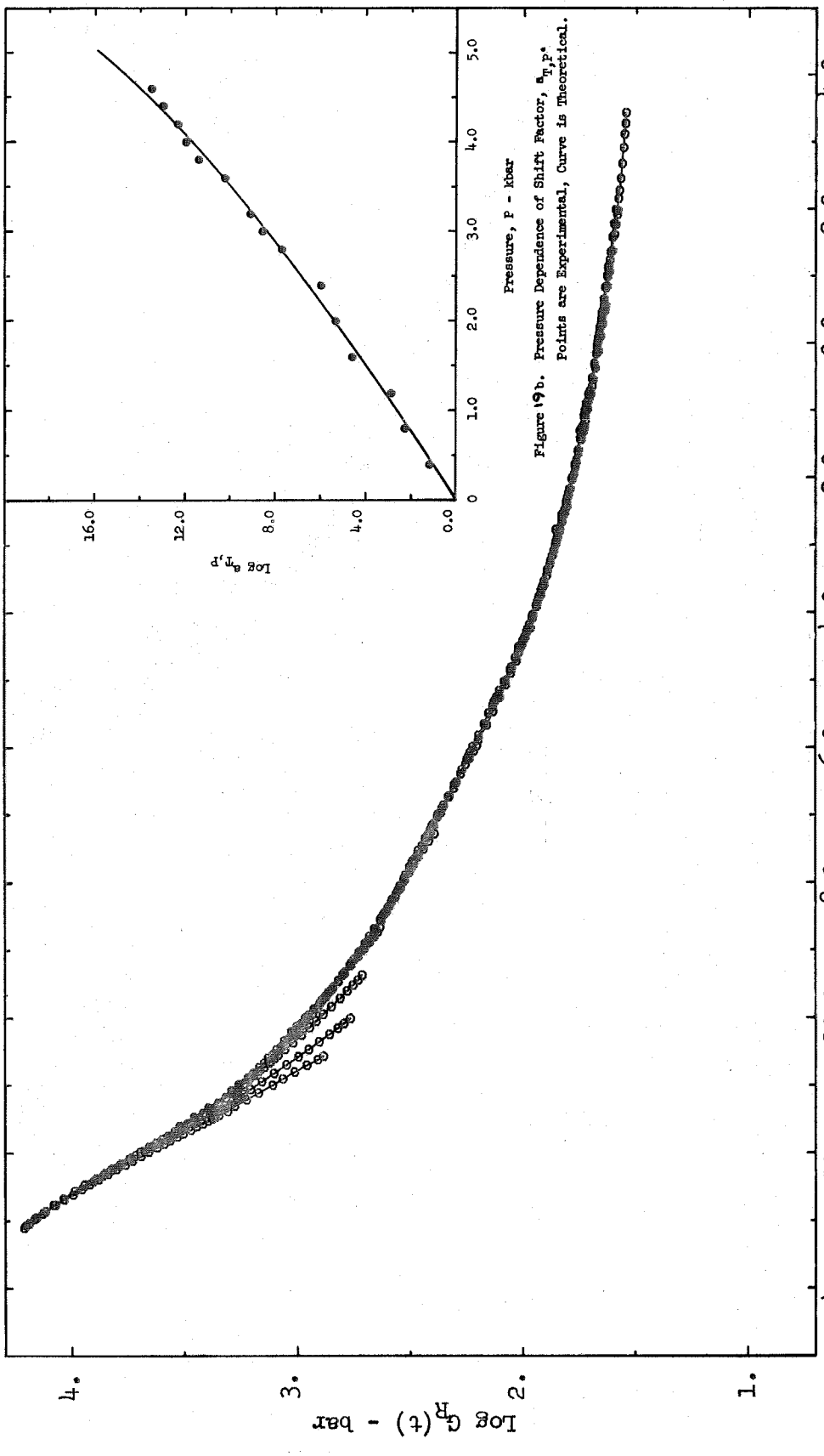

Figure 19a. Neoprene: Mastercurve. Shear Modulus, $G_R(t)$, Reduced by Shift Factors of Fig.19b to P=1.0

4. DISCUSSION AND CONCLUSIONS

In Chapter 3, information gathered over 3 decades of time, but covering a broad range of temperature and pressure, was brought into superposition by shifting along the logarithmic time axis. The resulting mastercurves were then proposed to represent material behavior over 13 decades of time at the reference temperature and pressure. The assumptions underlying this reduction scheme are: (1) the general effect of temperature and pressure on the rate of molecular rearrangement is to multiply all relaxation times by a common factor, $a_{T,P}$, where

$$a_{T,P} = \frac{\tau_p(T,P)}{\tau_p(T_o,P_o)} = \frac{\eta(T,P)T_o\rho_o}{\eta_b T\rho} \approx \frac{\eta(T,P)}{\eta_o(T_o,P_o)} \tag{71}$$

where $\tau_p(T,P)$ is the p'th relaxation time, and $\eta(T,P)$ is the steady-flow viscosity at temperature T and pressure P; and (2) the general effect of temperature and pressure on the moduli at fixed time is to change the configurational entropy and the internal energy of the system, by the factor, $d_{T,P}$, where

$$G^{T_o,P_o}(t/a_{T,P}) = d_{T,P}\, G^{T,P}(t) \tag{72}$$

The configurational entropy dominates the elastic, or equilibrium, response of the rubber, and

$$d_{T,P} = \rho_o T_o / \rho\, T\,, \quad \rho = \rho\,(T,P) \tag{73}$$

from the statistical theory of rubberlike elasticity. The internal energy dominates the elastic response of the glass, and some combination of the two control the elastic response in the transition region; we have no theory to guide us in these regions.

We now assume that the temperature and pressure dependence of the viscosity, Eq. (71), can be described by the temperature and pressure dependence of the free volume through the Doolittle equation

$$\eta = A_f \exp(B_f V_\phi / V_f), \quad V_\phi + V_f = V \tag{19}$$

where V_ϕ and V_f are the occupied and free volumes, respectively. We may then combine the Doolittle equation with Eq. (71) to obtain

$$\ln a_{T,P} = B_f \left[\frac{1}{f(T,P)} - \frac{1}{f(T_o, P_o)} \right] \tag{74}$$

where $f(T,P)$ is the fractional free volume,

$$f(T,P) = V_f / V \approx V_f / V_\phi \tag{75}$$

Since $V_f << V_\phi$. We now turn our attention to the effect of temperature and pressure on the fractional free volume, $f(T,P)$.

4.1 Effect of Temperature and Pressure on the Fractional Free Volume

Since we are interested in the change in the fractional free volume with temperature and pressure, we differentiate f to obtain

$$df = \left(\frac{\partial f}{\partial T}\right)_P dT + \left(\frac{\partial f}{\partial P}\right)_T dP \tag{76}$$

We now integrate Eq. (76), choosing the path which requires knowledge of the effect of pressure on the thermal expansivity of f. We thus have

$$\int_{T_o, P_o}^{T, P} df = \int_{T_o, P_o}^{T_o, P} \left(\frac{\partial f}{\partial P}\right)_{T_o} dP + \int_{T_o, P}^{T, P} \left(\frac{\partial f}{\partial T}\right)_P dT \tag{77}$$

It is obvious from Eq. (77) that equations of state $V = V(P, T)$ and $V_f = V_f(P, T)$ will be required to carry out the integration.

4.11 Equation of State for the Volume

We make use of the experimental fact,

$$\begin{aligned} K(T, P) &= K^*(T) + kP \\ K^*(T) &= K^*(T_o) \exp\left[-m\,\alpha^*(T - T_o)\right] \end{aligned} \tag{78}$$

where $K^*(T)$ is the zero pressure bulk modulus, α^* the zero pressure

thermal expansivity, and m and k are material parameters of the order of 5 and 10, respectively. It was shown in Section 1.6 that either the Murnaghan or the Tait equation may be obtained from Eq. (78), depending upon the definition of the compressibility. We choose the classical definition of the compressibility,

$$\beta = - \frac{1}{V} \left(\frac{\partial V}{\partial P}\right)_T \tag{79}$$

which, yields

$$V = V^* (1 + kP/K^*)^{-1/k} \tag{80}$$

when integrated with respect to Eq. (79), and is known as the Murnaghan equation; V^* is the volume at zero pressure. We next define the thermal expansivity at zero pressure as

$$\alpha^* = \frac{1}{V^*} \left(\frac{\partial V^*}{\partial T}\right)_P \tag{81}$$

Integrating Eq. (81) yields

$$V^* = V_o^* \exp [\alpha^*(T - T_o)] \approx V_o^* [1 + \alpha^*(T - T_o)] \tag{82}$$

where V_o^* is the volume at $P = 0$, $T = T_o$. In order to integrate Eq. (77), we need the pressure dependence of the thermal expansivity, $\alpha(P)$. Making use of Eqs. (80), and (78), we obtain

$$\alpha(P) = \frac{1}{V}\left(\frac{\partial V}{\partial T}\right)_P = \alpha^*\left[1 - \frac{mP}{K^* + kP}\right] \tag{83}$$

We now have all the volumetric relations necessary for integrating Eq. (77).

4.12 Equation of State for the Fractional Free Volume

We assume the temperature and pressure dependence of the free and occupied volumes to have the same functional form as the total volume described in Section 4.11. We further assume that $V_f << V$.

We now consider the partial differentials in Eq. (77). By Eq. (75)

$$\left(\frac{\partial f}{\partial T}\right)_P = \frac{1}{V}\left(\frac{\partial V_f}{\partial T}\right)_P - \frac{V_f}{V^2}\left(\frac{\partial V}{\partial T}\right)_P$$

$$= \alpha_f - f\alpha_r \approx \alpha_f \tag{84}$$

where α_f and α_r are the thermal expansivities of the free volume and rubber respectively. Since $V_f = V - V_\phi$, we have

$$\frac{1}{V}\left(\frac{\partial V_f}{\partial T}\right)_P = \frac{1}{V}\left(\frac{\partial V}{\partial T}\right)_P - \frac{1}{V}\left(\frac{\partial V_\phi}{\partial T}\right)_P \tag{85}$$

or

$$\alpha_f = \alpha_r - \alpha_\phi \tag{86}$$

where α_ϕ is the thermal expansivity of the occupied volume. Similarly, we find

$$\left(\frac{\partial f}{\partial P}\right)_T \approx \frac{1}{V}\left(\frac{\partial V_f}{\partial P}\right)_T = -\beta_f = \beta - \beta_r \tag{87}$$

or

$$\beta_f = \beta_r - \beta_\phi \tag{88}$$

4.13 Effect of Temperature and Pressure on the Fractional Free Volume

We may now substitute Eqs. (84) and (87) into Eq. (77) to obtain

$$\int_{T_o,P_o}^{T,P} df = -\int_{T_o,P_o}^{T,P} \beta_f(T_o)dP + \int_{T_o,P}^{T,P} \alpha_f(P)\, dT \tag{89}$$

or

$$f - f_o = -f_{T_o}(P) + f_P(T)$$

where f_o is the fractional free volume at the reference temperature and pressure. We first consider $f_{T_o}(P)$, and make use of Eqs. (80) and (89) to obtain

$$f_{T_o}(P) = \int_{P_o}^{P} \beta_r(T_o)\, dP - \int_{P_o}^{P} \beta_\phi(T_o)\, dP$$

$$= \frac{1}{k_r} \ln\left[1 + \frac{k_r P}{K_r^*}\right] - \frac{1}{k_\phi} \ln\left[1 + \frac{k_\phi P}{K_\phi^*}\right] \qquad (90)$$

where we have let $P_o = 0$. For $f_P(T)$ we obtain similarly

$$f_P(T) = \int_{T_o}^{T} \alpha_f(P)\, dT$$

$$= \alpha_f(P)\,[T - T_o] \qquad (91)$$

We assume the pressure dependence of $\alpha_f(P)$ to be described by Eq. (83). This implies that the parameter m of the total and occupied volumes are equal. This has been shown to be true for the rubbery and glassy states (37), and therefore should be a good assumption for the occupied volume.

Substituting Eq. (89) into Eq. (74) yields

$$\log a_{T,P} = \frac{B_f}{2.303\, f_o} \left[\frac{f_{T_o}(P) - f_P(T)}{f_o + f_P(T) - f_{T_o}(P)}\right] \qquad (92)$$

where $f_{T_o}(P)$ and $f_P(T)$ are given by Eqs. (90) and (91) respectively. If we set P equal to zero and T equal to T_g, the WLF equation, Eq. (25), is recovered. If we let $T = T_o$ and assume the

compressibility to be linear with pressure, $f_{T_o}(P) = \beta_f(P - P_o)$, we recover the Ferry-Stratton equation, Eq. (31).

Neither the Ferry-Stratton equation nor the O'Reilly equation, Eq. (38), were able to describe the experimental shift factors, $\log a_{T,P}$, presented in Chapter 3. It is usually assumed that the O'Reilly relationship is based on the Tait equation. This probably explains why neither the Tait nor the Murnagham equations have been applied to the free volume theory. If the Tait equation is properly applied, Eq. (90) is unchanged; the only difference is the values of the parameters k_r and k_ϕ, since they are evaluated differently for the Tait equation. Both equations describe the data quite well over the range of temperature and pressure used in this investigation.

4.14 Determination of the Expansivity and Compressibility of the Occupied Volume

When predicting the shift factors obtained from superposing isobaric stress relaxation segments measured at different temperatures, the parameters required for the $\log a_{T,P_o}$ equation are: B_f, f_o, α_r and α_ϕ. Of these only α_r can be measured independently. The common practice is to assume that $B_f = 1$. If one further assumes that $\alpha_\phi = \alpha_g$, f_o can be determined from fitting the data. This does not, in general, lead to a satisfactory description. One therefore varies both f_o and α_ϕ.

Conversely, when predicting the shift factors resulting from

superposing isothermal relaxation segments measured at different pressures, one needs the parameters: B_f, f_o, K_r^*, k_r, K_ϕ^* and k_ϕ. Here, K_r^* and k_r may be obtained independently. One could again proceed essentially as in the isobaric case.

When isobaric and isothermal measurements are combined, however, the situation changes. Since B_f and f_o must be the same in both sets of experiments, and since the mastercurves must coincide, it becomes possible to choose the appropriate values of B_f and f_o. The process is carried out by first assuming the parameters of the occupied volume to be identical to those of the glass. B_f, f_o, α_ϕ, k_ϕ, and K_ϕ^* are then determined using an iterative fitting procedure with the constraint that B_f and f_o, respectively, must be the same for the isobaric and isothermal mastercurves.

4.15 Comparison of Theoretical Prediction to Experimental Results

It is usually assumed that the thermal expansivity and compressibility of the occupied volume, α_ϕ and β_ϕ, are simply that of the glass. Based on this assumption, Eqs. (90-92) were applied to the shift factors, $\log a_{T,P}$, resulting from superposing the two mastercurves of Fig. 10a. It was possible to fit independently both $\log a_{T,P_o}$ and $\log a_{T_o,P}$ quite well with this assumption; however, the parameters B_f and f_o obtained from fitting the two sets of data were not equal. Since both mastercurves are reduced to the same

reference temperature and pressure, B_f and f_o must be constant. In order to make B_f and f_o, respectively, the same, it was necessary to conclude that $\alpha_\phi \neq \alpha_g$, nor $\beta_\phi \neq \beta_g$. By allowing α_ϕ and β_ϕ to vary, the best fit was obtained with the constraint that B_f and f_o be equal for the time-temperature and the time-pressure superposition. The resulting curves are plotted in Figs. 10b, 14b, and 19b; the values of the parameters used, together with the values of the glass, are reported in Table II. The point at which the experimental data deviate from the predicted response indicates the onset of glassy behavior.

Having fitted the parameters in Eq. (92) with the shift factors resulting from the mastercurves of Figs. 10a and 14a, the validity of the model was tested by predicting the time-temperature behavior at 1,000 and 2,000 bar. Using Eq. (83) to predict the effect of pressure on α_f (this is a fairly small correction), the predictions are plotted in Figs. 11b and 15b, along with the experimental points. The value of m was taken from data on polystyrene by Ouach and Simha (34). This value gave a satisfactory fit for the Viton, but overpredicted the Hypalon results. A satisfactory fit was obtained with half the value. This is consistent with the fact that pressure has twice the effect on Viton relative to Hypalon.

The three-dimensional character of Eq. (92) is displayed in Figs. 20 and 21 for the Hypalon and Viton respectively. The shape

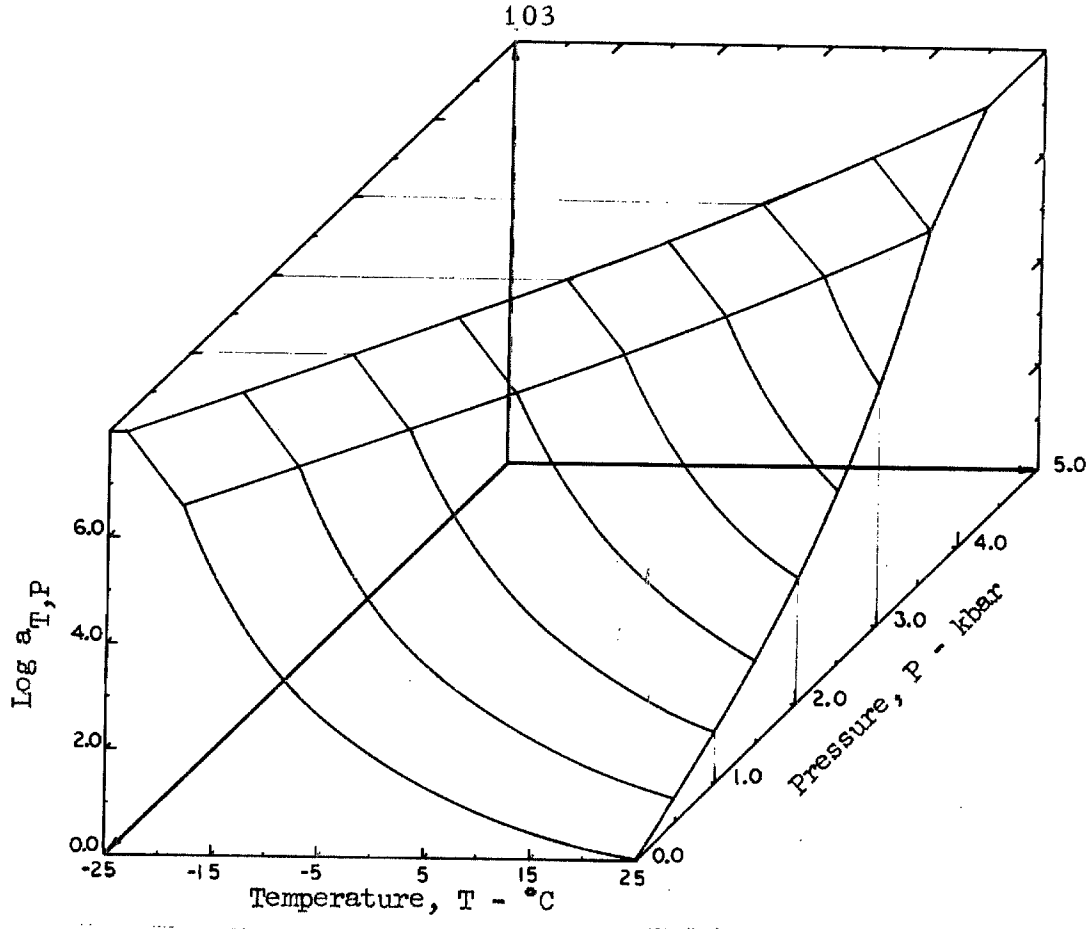

Figure 20. Hypalon-40: Shift Factor, log $a_{T,P}$, Dependence on Temperature and Pressure.

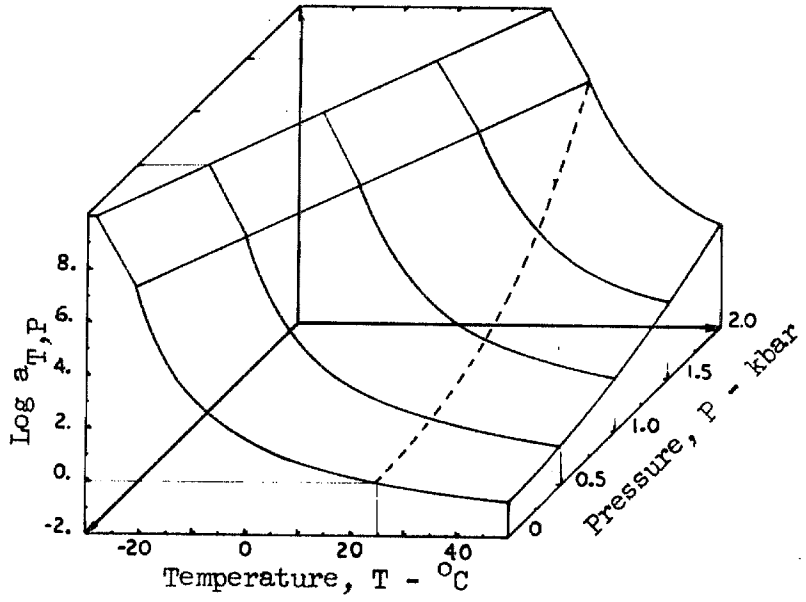

Figure 21. Viton-B: Shift Factor, log $a_{T,P}$, Dependence on Temperature and Pressure.

of the glassy behavior is mostly conjecture since little information was obtained in this region. It is seen that the inflection temperature, T_I, occurs at a constant value of log $a_{T,P}$. This is consistent with the experimental results, and implies that time-pressure superposition yields the same results as time-temperature superposition.

The intersection of the rubbery and glassy behavior is a straight line for the Viton, and is nearly a straight line for Hypalon. This implies that dT_g/dP is a constant for these materials over this range of temperature and pressure.

In order to check the applicability of Eq. (92) on a non-crosslinked polymer, the results of Zosel (43) on poly(vinylchloride) were fitted. The values of K_r^* and k_r were calculated from the compressibility data of Hellwege et al. (56). The results of applying Eq. (92) are displayed in Fig. 22, and the parameters are reported in Table II . Zosel was not able to fit the data with either the Ferry-Stratton or the O'Reilly equations.

The value of f_o reported in Table II is calculated by assuming T_g to be approximately T_I, and using the value of α_f shown. If α_f is assumed to be $(\alpha_r - \alpha_g)$, f_g is approximately 0.025 for both Hypalon and Viton. The time-temperature data can be fitted very well by assuming $\alpha_f = \alpha_r - \alpha_g$, since there is sufficient latitude in choosing B_f and f_o. However, in applying Eq. (92) to both the time-temperature and time-pressure data, these degrees of freedom are lost, and we must allow α_f to assume different values.

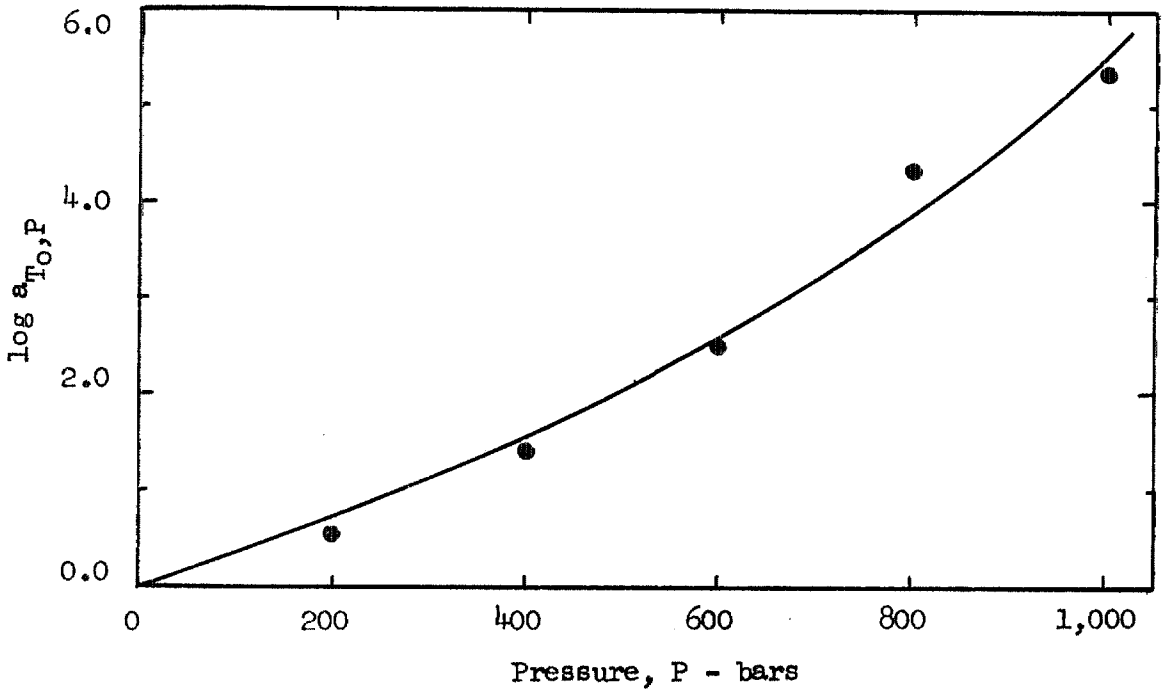

Figure 22. Application of Eq. (92) to the empirical shift factors of poly(vinylchloride)measured by Zosel (43).

The implication is that f_g is not 0.025 since α_f is not $\alpha_r - \alpha_g$.

We may not make any conclusions on the compressibility since we were forced to assume the effect of pressure on the Hypalon and Viton. The values of k_ϕ reported for the Hypalon and Viton are high, but could easily result from the assumed behavior of the rubber. The value for Neoprene is also high, but may result from the high filler content of the system. The value of 12.5 for PVC is quite satisfactory. Unfortunately, the data of Hellwege did not cover the glassy region. The compressibility of PVC was also measured by Weir (55) up to 10 kbar pressure. In the rubbery

TABLE II

Material Parameters

Parameter	Hypalon	Viton	Neoprene	PVC
f_{25}	0.040	0.0398	0.058	0.036
$f_o(\alpha_f, T_I)$	.012	0.010	---	---
B_f	0.246	0.202	1.34	0.428
$\alpha_r(10)^4 {}^oC^{-1}$	7.3	7.2	7.25	---
α_g	4.4	4.1	---	---
α_f	6.66	6.73	---	---
k_r	10.8	10.8	10.8	7.7
k_g	11.1	11.1	11.1	---
k_ϕ	18.2	38.0	16.4	12.5
$K_r*(10)^{-4}$bar	2.30	2.30	2.30	2.40
$K_g*(10)^{-4}$bar	2.64	2.64	2.64	---
$K*(10)^{-4}$bar	3.23	3.46	3.51	5.38
m	3.2	6.5	---	---

region sufficient data were not available to obtain a value of K_r; plotting the data in terms of K yielded $k_g = 3.9$. This is very low for the slope in the glassy region and is possibly in error. We expect the slope to be higher for the glass than the rubber, since the material has a finite compressibility. As a result we may not

make any absolute conclusions on the nature of β_f relative to β_r and β_g, but it appears from the results on α_f, that they are probably not simply related. We may conclude, however, that the Murnaghan or Tait equations adequately describe the behavior of the fractional free volume.

4.2 Conclusions and Recommendations

The work presented here has demonstrated that a proper extension of the free volume theory provides a satisfactory way to account for the effect of pressure on the relaxational properties of polymeric materials. Previous attempts to extend the free volume theory either failed to take into account the pressure dependence of the compressibility or introduced it in an incorrect way. It is shown in this investigation that either of two closely related expressions, the equations of Tait and of Murnagham, will lead to the desired result.

It is an important aspect of the work reported here that the use of pressure in addition to temperature allows the removal of some ambiguities in the free volume theory which could not be resolved in any other way. The parameters α_f, B_f and f_o in the WLF equation can not be determined from shift factors resulting from time-temperature superposition alone, since the system is not conpletely determined. By employing the additional variable of pressure, these ambiguities are removed. Since time-temperature-

pressure superposition must predict the same master curve, no degree of freedom remains in both shifting the data and in fitting the log $a_{T,P}$ equation. It was found that B_f is generally not equal to unity and that α_f is not equal to $\alpha_r - \alpha_g$.

This investigation was limited to elastomers having relatively low pressure transitions due to problems with the triggering mechanism. The investigation should be extended to a number of other polymers, including the technologically important elastomers such as natural rubber and SBR; this extension should further include compressibility measurements of these materials.

APPENDIX A

DET NO.	NO. REQD	MATERIAL AND DESCRIPTION
		CALIFORNIA INSTITUTE OF TECHNOLOGY
		CHEMICAL ENGINEERING | R. FILLER & E.X 1675
		STRESS RELAXOMETER | SHT 1 OF 6
602	1	'T' PIN
601	1	SOLENOID BRACKET
505	1	STRAIN GAGE ASSY
504	4	CLEVIS SCR
503	1	CLEVIS
502		SPECIMEN HOLDER
501	1	END CAP, TOP
403		SPACER
402	1	LATCH
401	1	END CAP, BOTTOM
301	1	INNER CYLINDER
201	1	OUTTER CYLINDER
110	1	#1-72 x 1/8 FLAT PT. SET SCR
109	1	3/32 O.D. TUBE
108	2	#1-72 x 3/16 BUTTON HD. SOC. CAP SCR.
107	1	ELECTRO-MECHANISMS SP-37-6V SOLND.
106	1	CENTURY SPRING CAT N.B 892
105	1	3/32 DIA x 7/8 DOWEL PIN
104	2	3/16 O.D. x .032 WL x 3/8 BRASS TUBE
103	1	1/8 DIA x 7/8 DOWEL PIN
102	1	1/16 DIA x 1/8 DOWEL PIN
101	1	RELAXOMETER ASSY

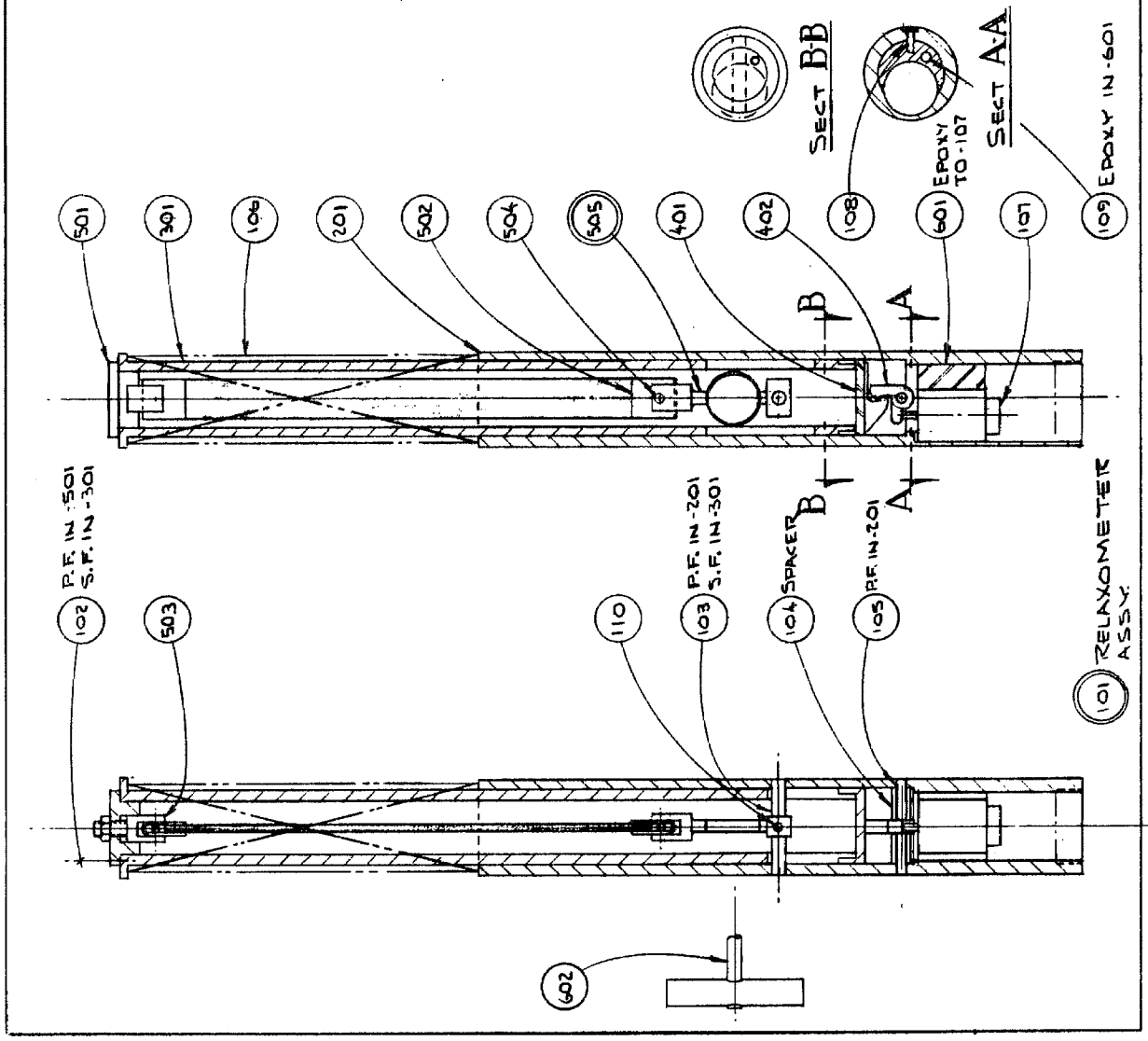

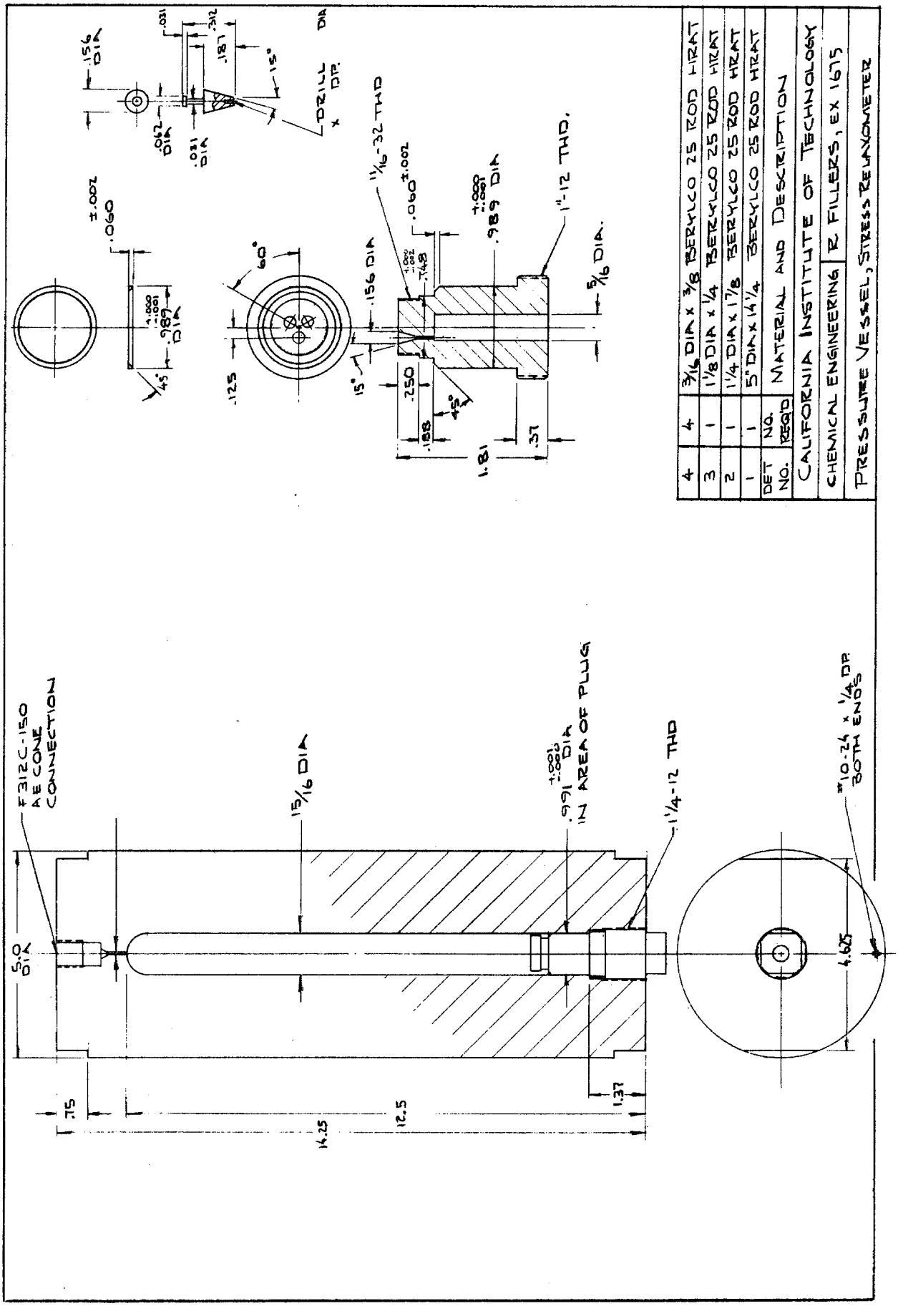
4 4 3/16 DIA x 3/8 BERYLCO 25 ROD HRAT
3 1 1/8 DIA x 1/4 BERYLCO 25 ROD HRAT
2 1 1 1/4 DIA x 1 7/8 BERYLCO 25 ROD HRAT
1 1 5" DIA x 14 1/4 BERYLCO 25 ROD HRAT
DET NO. NO. REQ'D MATERIAL AND DESCRIPTION
CALIFORNIA INSTITUTE OF TECHNOLOGY
CHEMICAL ENGINEERING & FILLERS, EX 1675
PRESSURE VESSEL, STRESS RELAXOMETER
F312C-150 AE CONE CONNECTION
15/16 DIA
.991 DIA AREA OF PLUG
1 1/4-12 THD
#10-24 x 1/4 DP BOTH ENDS
5.0 DIA
4.625
.75
14.25
12.5
1.37
1 1/16-32 THD
1"-12 THD.
5/16 DIA.
.989 DIA
.156 DIA
60°
15°
45°
.250
.188
1.81
.37
.125
.060 ±.002
.060 ±.002
.748
.156 DIA
.042 DIA
.031 DIA
.187
.312
.031
15°
DRILL DP x DIA

APPENDIX B

The EPDM elastomer was prepared by curing 100 parts U.S. Rubber Co. Royalene 301T with 3 phr Di-cup R. Royalene 301T is an ethylene-propylene copolymer containing a controlled amount of non-conjugated diene. Di-cup R is a 98 - 99% active dicumyl peroxide manufactured by Hercules, Inc.

The reduced shear moduli, $G_r(t)$, are plotted in Figs. 23 and 24. Fig. 23 shows the results of measurements at 25.0 ^{o}C as a function of pressure. The inability to apply time-pressure superposition to the segments is exhibited by the extreme downward curvature of the ends of the segments, and is particularly evidenced in segments (1 - 4). The lack of superposition is again found for the measurements at 1.0 bar as a function of temperature reported in Fig. 24. The segments measured as a function of temperature are seen to display similar behavior to the segments measured as a function of pressure. In both cases, the relaxation times are affected differently by either a change in temperature, or a change in pressure.

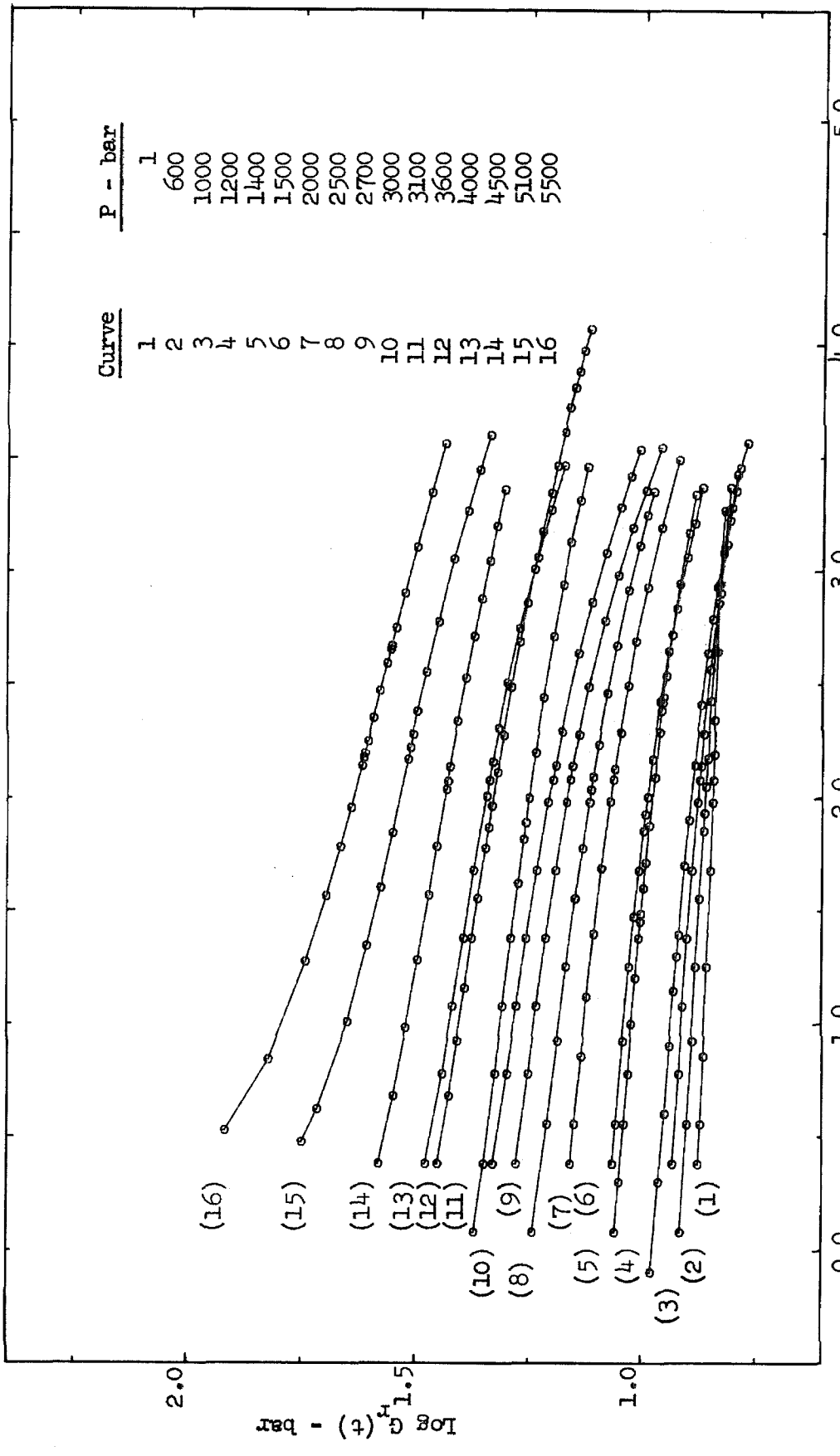

Figure 23. EPDM: Shear Modulus, $G_r(t)$, at T = 25.0 °C and Pressures Indicated.

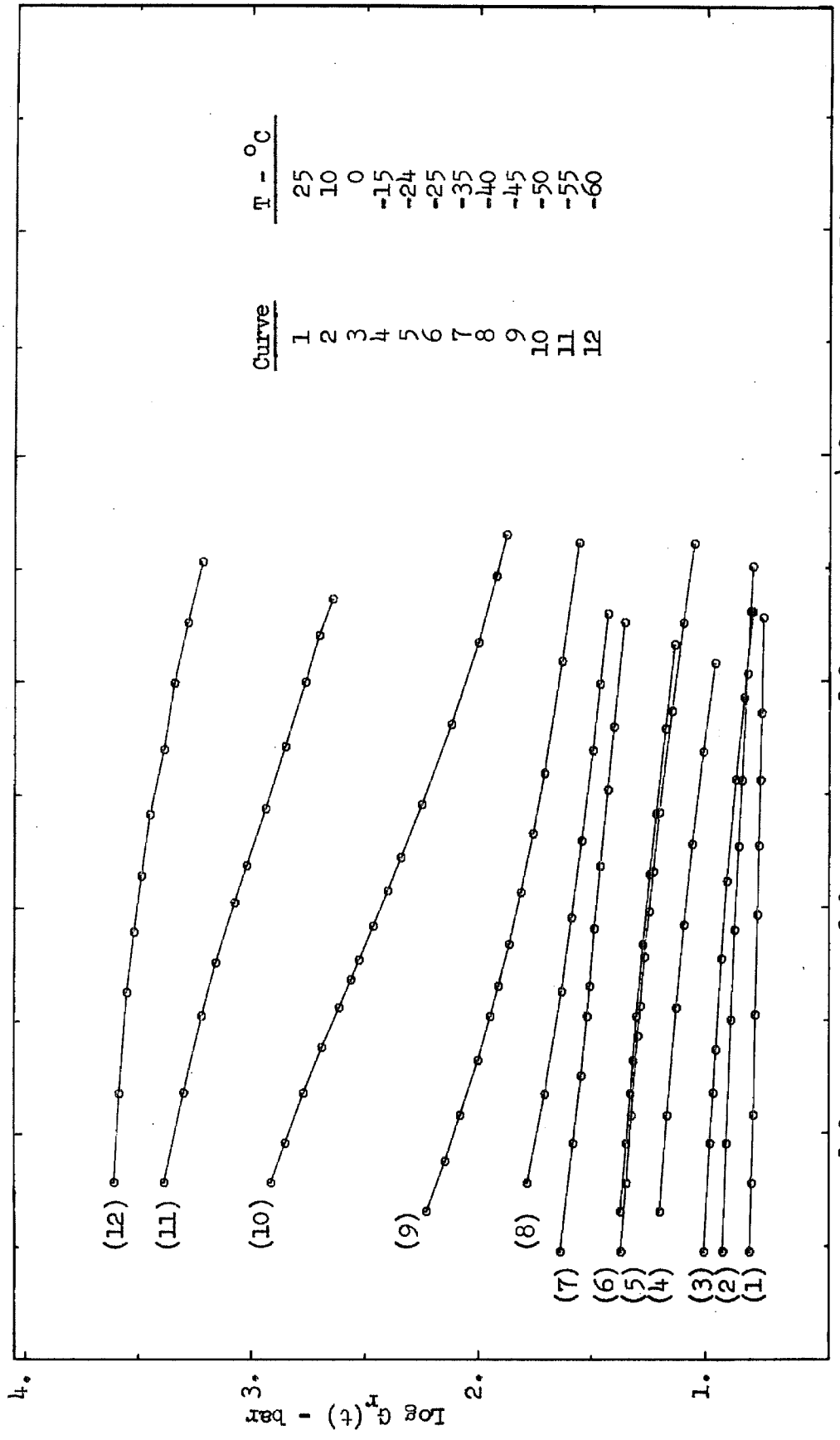

Figure 24. EPDM: Shear Modulus, $G_r(t)$, at P = 1.0 bar and Temperatures Indicated.

References

1. R. O. Davies and G. O. Jones, Proc. Roy. Soc. (London). 217A:26 (1953).

2. L. Boltzmann, Sitzungsber. Kgl. Akad. Wiss. Wien, Math.-Naturw. Classe (2A) 70:275 (1874); Pogg. Ann. Phys. 7:624 (1876).

3. J. D. Ferry, Viscoelastic Properties of Polymers, Wiley, New York, (1970).

4. B. D. Coleman and W. Noll, Rev. Mod. Phys. 33:239 (1961).

5. P. E. Rouse, Jr., J. Chem, Phys. 21:1272 (1953).

6. B. H. Zimm, J. Chem. Phys. 24:269 (1956).

7. J. D. Ferry, R. F. Landel, and M. L. Williams, J. Applied Phys. 26:359 (1955).

8. H. Leaderman, Elastic and Creep Properties of Filamentous Materials and Other High Polymers, The Textile Foundation, Washington, 1943.

9. A. V. Tobolsky and R. D. Andrews, J. Chem. Phys. 11:125 (1943).

10. M. L. Williams, R. F. Landel and J. O. Ferry, J. Amer. Chem. Soc. 77:3401 (1955).

11. N. G. McCrum and E. L. Morris, Proc. Roy. Soc. A281:258 (1964).

12. N. G. McCrum, J. Poly. Sci. A2:3951 (1964).

13. H. Vogel, Physik. Z. 22:645 (1921).

14. G. Tamman and G. Hesse, Z. anorg. allg. Chem. 156:245 (1926).

15. H. Eyring, J. Chem. Phys. 4:233 (1936).

16. A. J. Batchinski, Z. Phys. Chem. 84:644 (1913).

17. A. K. Doolittle, J. Applied Phys. 22:1471 (1951); 28:901 (1957).

18. D. Turnbull and M.H. Cohen, J. Chem. Phys. 31:1164 (1959); 34:120 (1961); 52:3038 (1969).

19. R. Simha and R. F. Boyer, J. Chem. Phys. 37:1003 (1962).

20. T. G. Fox and P. J. Flory, J. Applied Phys. 21:381 (1950).

21. R. F. Boyer, Rubber Chem and Tech. 36:1303 (1963).

22. D. H. Kaelble, "Free Volume and Polymer Rheology," Chapt. 5 in Rheology, Vol. 5 (Editor F. R. Eirich), Academic Press, New York (1969).

23. M. C. Shen and A. Eisenberg, Progress in Solid State Chemistry, Vol. 3, Pergamon Press, Oxford & New York (1966).

24. P. B. Macedo and T. A. Litovitz, J. Chem. Phys. 42:245 (1965).

25. J. Naghizadeh, J. Applied Phys. 35:1162 (1964).

26. R. O. Davies and G. O. Jones, Adv. in Phys. 2:370 (1953).

27. I. Prigogine and R. Defay, Chemical Thermodynamics, Longmans, Green & Co., London (1954).

28. M. Goldstein, J. Chem Phys. 39:3369 (1963).

29. A. B. Bestul and S. S. Chang, J. Chem Phys. 40:378 (1964).

30. J. H. Gibbs and E. A. DiMarzio, J. Chem. Phys. 28:373 (1958).

31. G. Adams and J. H. Gibbs, J. Chem. Phys. 43:139 (1965).

32. P. W. Bridgeman, The Physics of High Pressure, G. Bill and Sons, London (1949).

33. H. Breuer and G. Rehage, Kolloid-Z. Z. Polymere 216-217:159 (1967).

34. A. Quach and R. Simha, J. Applied Phys. 42:4592 (1971).

35. J. D. Ferry and R. A. Stratton, Kolloid-Z 171:107 (1960).

36. L. A. Wood, J. Poly. Sci. B2:703 (1969).

37. P. J. Blatz, "On the Thermostatic Behavior of Elastomers," Polymer Networks:Structural and Mechanical Properties (Ed. by A. J. Chompff) Plenum Press, New York, p. 23 (1971).

38. J. M. O'Reilly, J. Poly. Sci. 57:429 (1962).

39. J. E. McKinney, H. V. Belcher, and R. S. Marvin, Trans. Soc. Rheology 4:347 (1960).

40. R. S. Marvin and J. E. McKinney, "Volume Relaxation in Amorphous Polymers," in Physical Acoustics, Vol. 2B (Editor W. P. Mason), Academic Press, 165 (1965).

41. S. V. Radcliff, "Effects of Hydrostatic Pressure on the Deformation and Fracture of Polymers," in Deformation and Fracture of High Polymers (Ed. by H. H. Kausch, J. H. Hassel and R. I. Jaffee) Plenum Press, New York p. 191 (1972).

42. M. S. Patterson, J. Applied Phys. 35:176 (1961).

43. A. Zosel, Kolloid-Z 199:113 (1964).

44. E. Jones and D. Tabor, Polymer 14:617 (1973); 14:623 (1973); 14:629 (1973).

45. P. R. Billinghurst and D. Tabor, Polymer 12:101 (1971).

46. K. L. DeVries and D. K. Backman, J. Poly. Sci. 9:717 (1971).

47. D. M. Warschauer and W. Paul, Rev. Scientific Instru. 29:675 (1958).

48. S. E. Babbs & G. J. Scott, Rev. Sci. Inst. 36:1456 (1965).

49. W. G. Schlinger & B. H. Sage, Industrial and Eng. Chem. 42:2158 (1950).

50. J. R. Richards, R. G. Manche, J. D. Ferry, Poly Letters 2:197 (1964).

51. F. Haaf and P. R. Johnson, Rubber Chem and Tech. 44:1410 (1971).

52. A. C. Stevenson, "Neoprene, Hypalon, and Fluoroelastomers," in Vulcanization of Elastomers (Ed. by G. Alliger and I. J. Sjothun), Reinhold Publishing Co., New York., p. 265, (1964).

53. N. I. Shishkin, Soviet Phys. Solid State Phys. 2:322 (1960).

54. V. Bianchi, A. Turturro, and G. Basile, J. Chem. Phys 71:3555 (1967).

55. C. E. Weir, J. Res. Nat. Bureau Stds. 46:207 (1951); 53:245 (1954).

56. K. H. Hellwege, W. Knappe, and P. Lehmann, Kolloid-Z 183: 110 (1961).

57. S. C. Sharda, "Thermodynamic Behavior of Rubbers," Ph. D. Thesis, California Institute of Technology, Pasadena, California, 1974.